Supporting Information for:

Phenyl substitution of cationic *bis*-cyclometalated iridium(III) complexes for iTMC-LEECs†

Kristin J. Suhr,[a] Lyndon D. Bastatas,[b] Yulong Shen,[b] Lauren A. Mitchell,[a] Gary A. Frazier,[b] David W. Taylor,[b] Jason D. Slinker*[b] and Bradley J. Holliday[c]

[a] *Department of Chemistry, The University of Texas at Austin, Austin, TX 78712, USA. *E-mail: bholliday@cm.utexas.edu*
[b] *Department of Physics, The University of Texas at Dallas, 800 W. Campbell Rd, Richardson, TX 75080, USA. *E-mail: slinker@utdallas.edu*
[c] *Unaffiliated*

Supporting Information Table of Contents

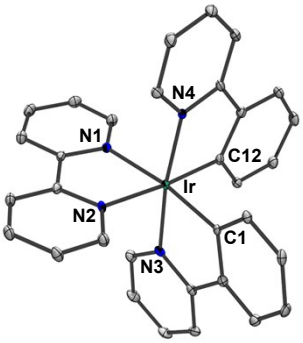

Fig. S1 ORTEP diagram of **C0**. Labels for selected atoms are shown. Thermal ellipsoids are drawn at a 30% probability level. Hydrogen atoms and the PF_6 counterion are omitted for clarity.

Table S1 Crystal data and structure refinement for **C0**

CCDC number	1453922
Empirical formula	$C_{32}H_{24}F_6IrN_4P$
Formula weight	801.72
Temperature (K)	100(2)
Wavelength (Å)	1.54184
Crystal system	Orthorhombic
Space group	*Pbca*
a (Å)	10.8560(7)
b (Å)	15.7756(8)
c (Å)	33.3846(7)
α (°)	90
β (°)	90
γ (°)	90
Volume (Å^3)	5717.4(5)
Z	8
Density (calculated) (Mg/m^3)	1.863
Absorption coefficient (mm^{-1})	10.194
F(000)	3120
Crystal size (mm^3)	0.28 x 0.06 x 0.04
Theta range for data collection (°)	2.65 to 74.17
Index ranges	$-13 \leq h \leq 6$
	$-19 \leq k \leq 13$
	$-41 \leq l \leq 29$
Reflections collected	13568
Independent reflections	5644 [R(int) = 0.0244]
Completeness to theta = 67.68°	99.8%
Refinement method	Full-matrix least-squares on F^2
Data / restraints / parameters	5644 / 0 / 397
Goodness-of-fit on F^2	1.054
Final *R* indices [$I > 2\sigma(I)$]	$R1 = 0.0247$, $wR2 = 0.0589$
R indices (all data)	$R1 = 0.0314$, $wR2 = 0.0628$
Largest diff. peak and hole (e.Å^{-3})	0.807 and -1.002

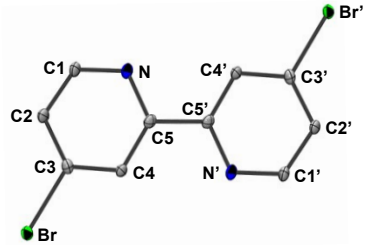

Fig. S2 ORTEP diagram of 4,4'-dibromo-2,2'-bipyridine. Thermal ellipsoids are drawn at a 30% probability level. Hydrogen atoms are omitted for clarity. The molecule resides around a crystallographic inversion center at ½, ½, ½. Atoms with labels appended by a ' are related by 1-x, 1-y, 1-z.

Table S2 Crystal data and structure refinement for 4,4'-dibromo-2,2'-bipyridine

CCDC number	1054651
Empirical formula	$C_{10}H_6Br_2N_2$
Formula weight	313.99
Temperature (K)	100(2)
Wavelength (Å)	0.71075
Crystal system	Monoclinic
Space group	$P2_1/n$
a (Å)	3.9238(11)
b (Å)	15.660(5)
c (Å)	7.824(2)
α (°)	90
β (°)	93.273(9)
γ (°)	90
Volume (Å^3)	480.0(2)
Z	2
Density (calculated) (Mg/m^3)	2.173
Absorption coefficient (mm^{-1})	8.400
F(000)	300
Crystal size (mm^3)	0.23 x 0.06 x 0.01
Theta range for data collection (°)	3.68 to 24.97
Index ranges	$-4 \leq h \leq 4$
	$-18 \leq k \leq 15$
	$-9 \leq l \leq 8$
Reflections collected	5251
Independent reflections	828 [R(int) = 0.1668]
Completeness to theta = 25.24°	95.0%
Refinement method	Full-matrix least-squares on F^2
Data / restraints / parameters	828 / 0 / 64
Goodness-of-fit on F^2	1.101
Final R indices [$I > 2\sigma(I)$]	$R1$ = 0.0488, $wR2$ = 0.1305
R indices (all data)	$R1$ = 0.0528, $wR2$ = 0.1351
Largest diff. peak and hole (e.Å^{-3})	1.830 and -1.186

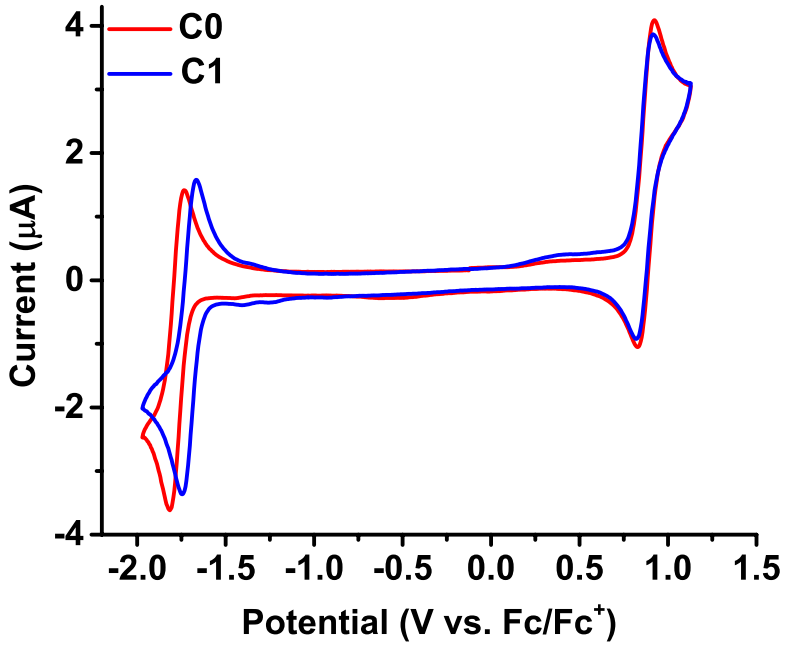

Fig. S3 Electrochemical CVs (2nd scans) of **C0** and **C1** (1 mM) in dry acetonitrile and 0.1 M $TBAPF_6$ at a scan rate of 0.1 V/s. **C0** and **C1** have identical oxidation onsets (HOMOs) because both complexes have the same **PhPy** cyclometalating ligand. The reduction onsets (LUMOs) demonstrate that the ancillary ligand **DiPhBipy** (blue, **C1**) is easier to reduce than **Bipy** (red, **C0**).

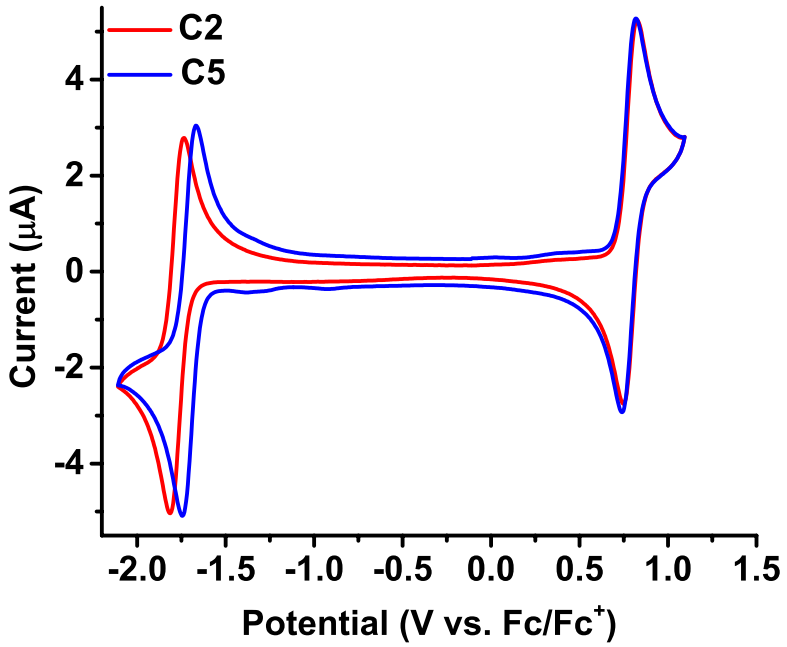

Fig. S4 Electrochemical CVs (2nd scans) of **C2** and **C5** (1 mM) in dry acetonitrile and 0.1 M $TBAPF_6$ at a scan rate of 0.1 V/s. **C2** and **C5** have identical oxidation onsets (HOMOs) because both complexes have the same **BiPhPy** cyclometalating ligand. The reduction onsets (LUMOs) demonstrate that the ancillary ligand **DiPhBipy** (blue, **C5**) is easier to reduce than **Bipy** (red, **C2**).

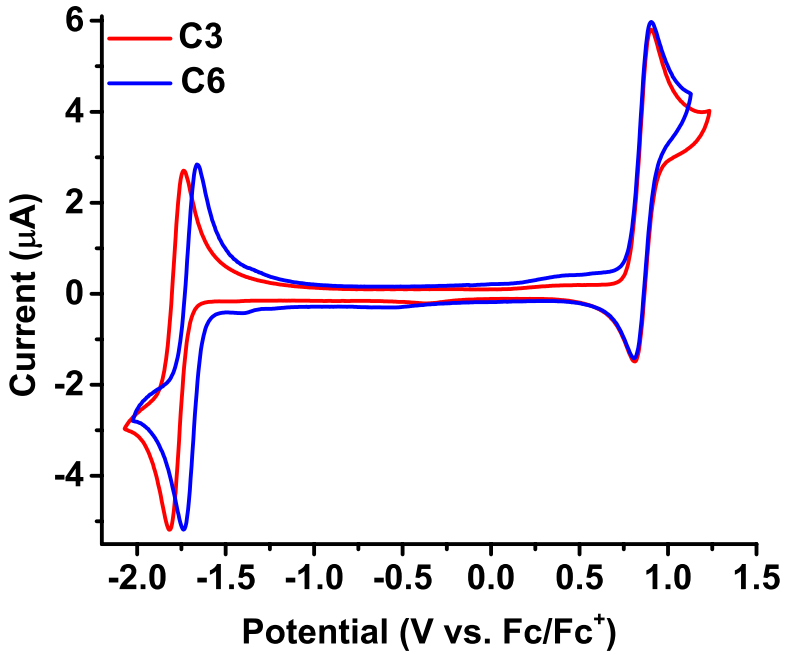

Fig. S5 Electrochemical CVs (2nd scans) of **C3** and **C6** (1 mM) in dry acetonitrile and 0.1 M $TBAPF_6$ at a scan rate of 0.1 V/s. **C3** and **C6** have identical oxidation onsets (HOMOs) because both complexes have the same **DiPhPy** cyclometalating ligand. The reduction onsets (LUMOs) demonstrate that the ancillary ligand **DiPhBipy** (blue, **C6**) is easier to reduce than **Bipy** (red, **C3**).

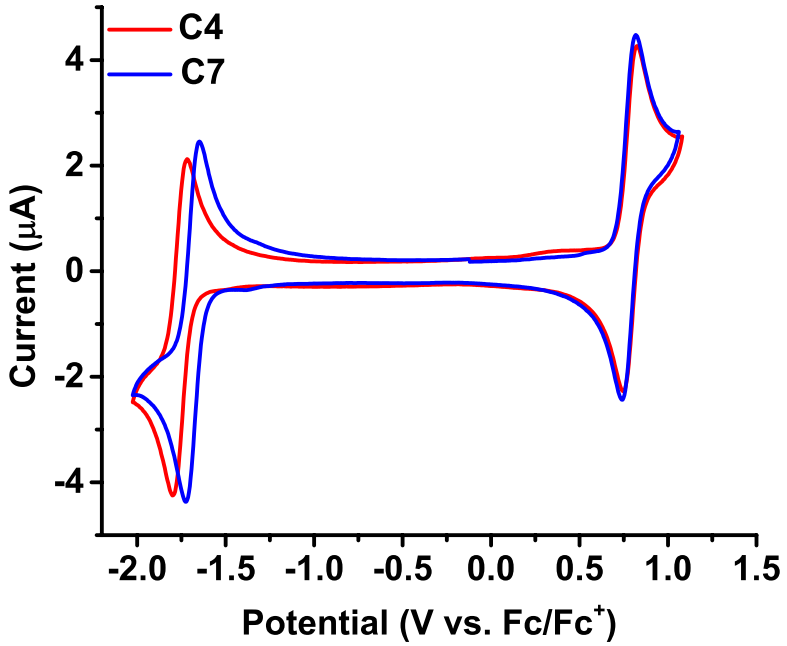

Fig. S6 Electrochemical CVs (2nd scans) of **C4** and **C7** (1 mM) in dry acetonitrile and 0.1 M $TBAPF_6$ at a scan rate of 0.1 V/s. **C4** and **C7** have identical oxidation onsets (HOMOs) because both complexes have the same **BiPhPhPy** cyclometalating ligand. The reduction onsets (LUMOs) demonstrate that the ancillary ligand **DiPhBipy** (blue, **C7**) is easier to reduce than **Bipy** (red, **C4**).

Table S3 UV-Vis absorption peaks and molar absorptivities of **C0–C7**

	λ_{abs} (nm) [ε (10^3 M^{-1} cm^{-1})][a]
C0	257* (48.4); 268* (47.7); 308sh (22.6); 336 (9.7); 356 (7.4); 381 (7.0); 409 (4.2); 467 (0.9); 491sh (0.6)
C1	267* (55.7); 286sh (47.6); 320sh (22.7); 342 (11.3); 367 (10.3); 385 (9.5); 416sh (3.7); 468 (1.2); 492sh (1.0)
C2	276* (89.7); 290sh (69.5); 313sh (30.1); 338 (12.1); 382 (6.9); 418 (4.8); 474 (0.9); 498sh (0.7)
C3	268* (66.9); 278sh (62.1); 307sh (34.6); 321sh (27.0); 339 (20.1); 381 (9.2); 466 (1.1); 497sh (0.4)
C4	268sh (91.3); 278* (98.1); 307sh (45.0); 339 (19.4); 379 (8.1); 473 (1.2)
C5	275 (95.6); 284* (96.4); 322sh (30.3); 343 (15.4); 365 (13.0); 387 (11.2); 422 (4.7); 478 (1.2); 500sh (1.1)
C6	255sh (77.9); 270* (91.9); 316sh (42.8); 339 (25.2); 384 (14.6); 466 (1.9); 496sh (1.2)
C7	271sh (119.3); 280* (123.6); 317sh (46.3); 343 (24.7); 387 (13.5); 474 (1.8); 502sh (1.2)

[a] Shoulders in the absorption peak are denoted with sh; * denotes the λ_{max} of absorption; the molar absorptivity of each peak is in parentheses after the peak wavelength.

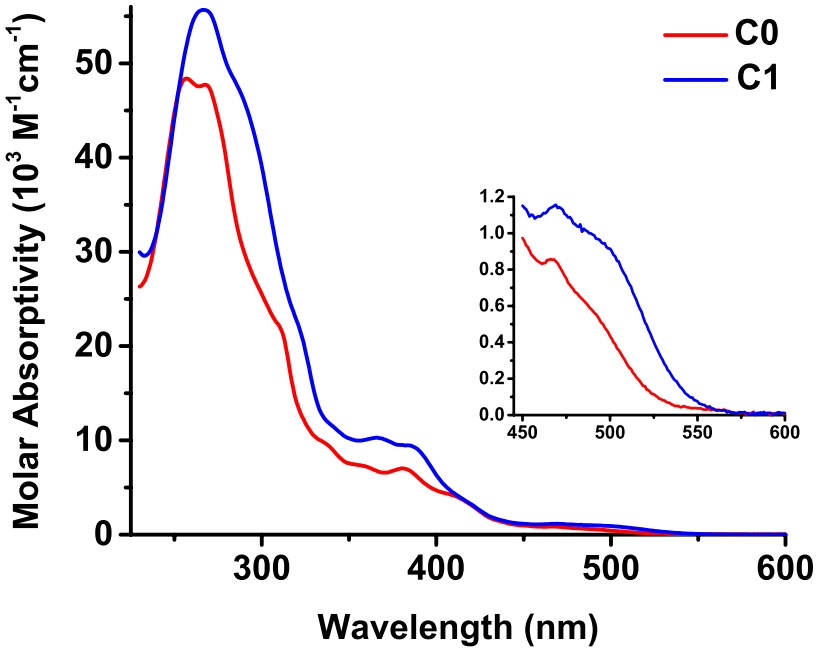

Fig. S7 UV-Vis absorption spectra of **C0** and **C1** in DCM at room temperature. Inset: expansion of triplet state absorption bands in the region of 450 to 600 nm. **C0** and **C1** have the same cyclometalating ligand (**PhPy**), however the addition of blocking phenyls to the ancillary ligand, **DiPhBipy** (blue, **C1**), allows for increased absorption across the spectrum.

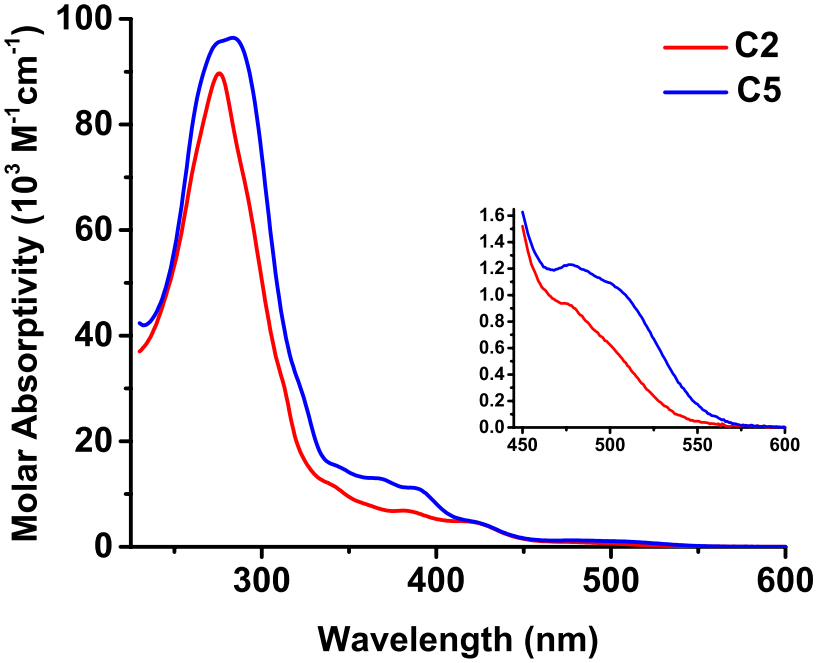

Fig. S8 UV-Vis absorption spectra of **C2** and **C5** in DCM at room temperature. Inset: expansion of triplet state absorption bands in the region of 450 to 600 nm. **C2** and **C5** have the same cyclometalating ligand (**BiPhPy**), however the addition of blocking phenyls to the ancillary ligand, **DiPhBipy** (blue, **C5**), allows for increased absorption across the spectrum.

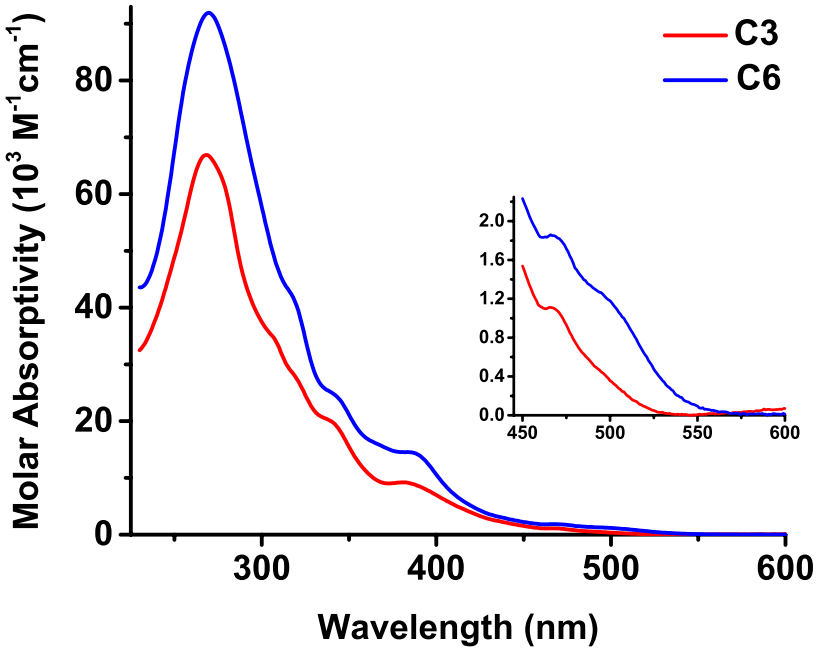

Fig. S9 UV-Vis absorption spectra of **C3** and **C6** in DCM at room temperature. Inset: expansion of triplet state absorption bands in the region of 450 to 600 nm. **C3** and **C6** have the same cyclometalating ligand (**DiPhPy**), however the addition of blocking phenyls to the ancillary ligand, **DiPhBipy** (blue, **C6**), allows for increased absorption across the spectrum.

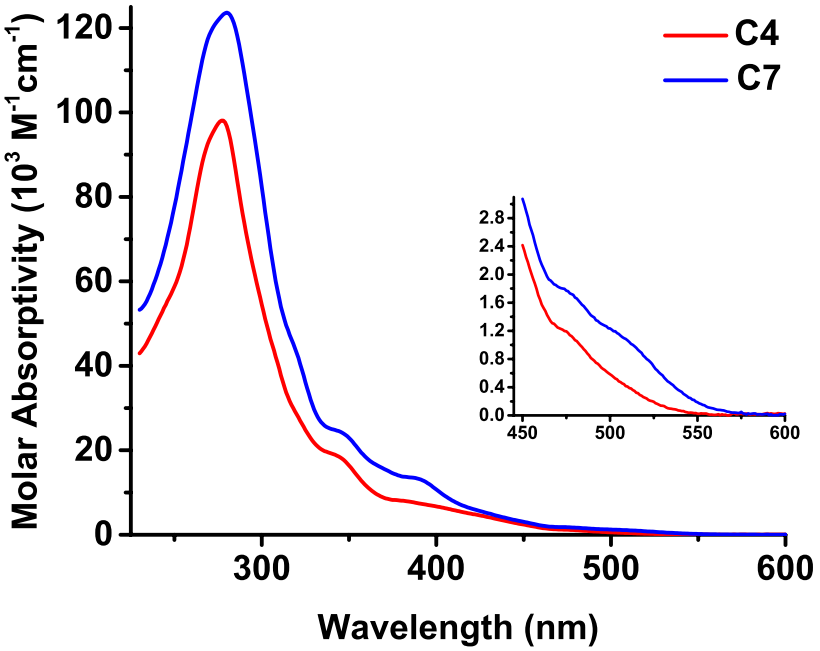

Fig. S10 UV-Vis absorption spectra of **C4** and **C7** in DCM at room temperature. Inset: expansion of triplet state absorption bands in the region of 450 to 600 nm. **C4** and **C7** have the same cyclometalating ligand (**BiPhPhPy**), however the addition of blocking phenyls to the ancillary ligand, **DiPhBipy** (blue, **C7**), allows for increased absorption across the spectrum.

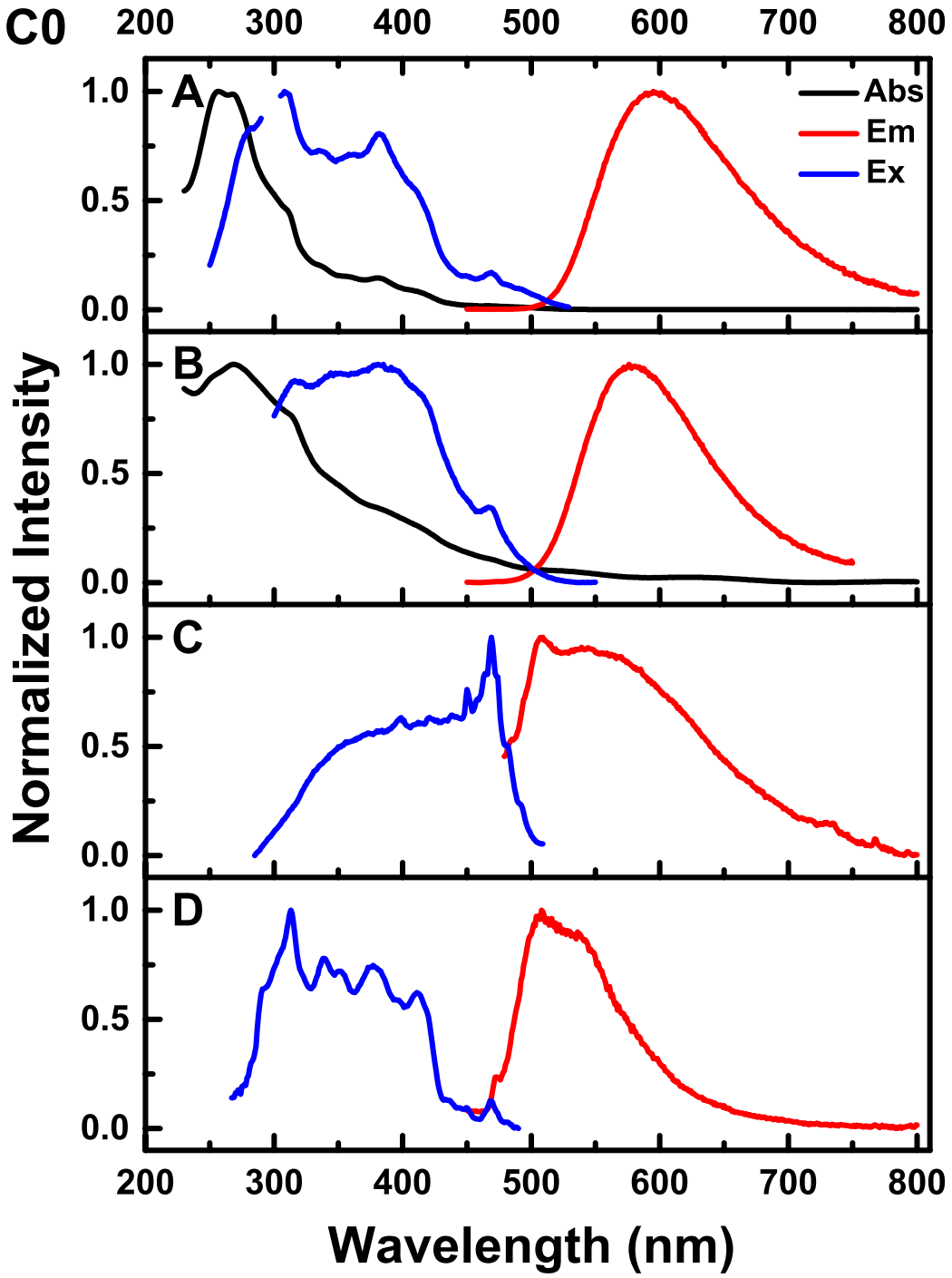

Fig. S11 Absorbance (black), photoluminescence excitation (blue), and emission (red) spectra of **C0**. A) Solution: DCM, 298 K, a 380 UV longpass optical filter was used for this emission profile; B) Dropcast Film: Evaporated from a concentrated solution in DCM, 298 K; C) Solid: 298 K; D) Frozen: 2-MeTHF, 77 K, a 380 UV longpass optical filter was used for this emission profile. The break in the solution excitation spectrum signifies an omitted peak due to half the emission wavelength. Both the broad, featureless emission peaks (red) and the rigidochromic effect present in the frozen state (D) are indicative of MLCT emission.

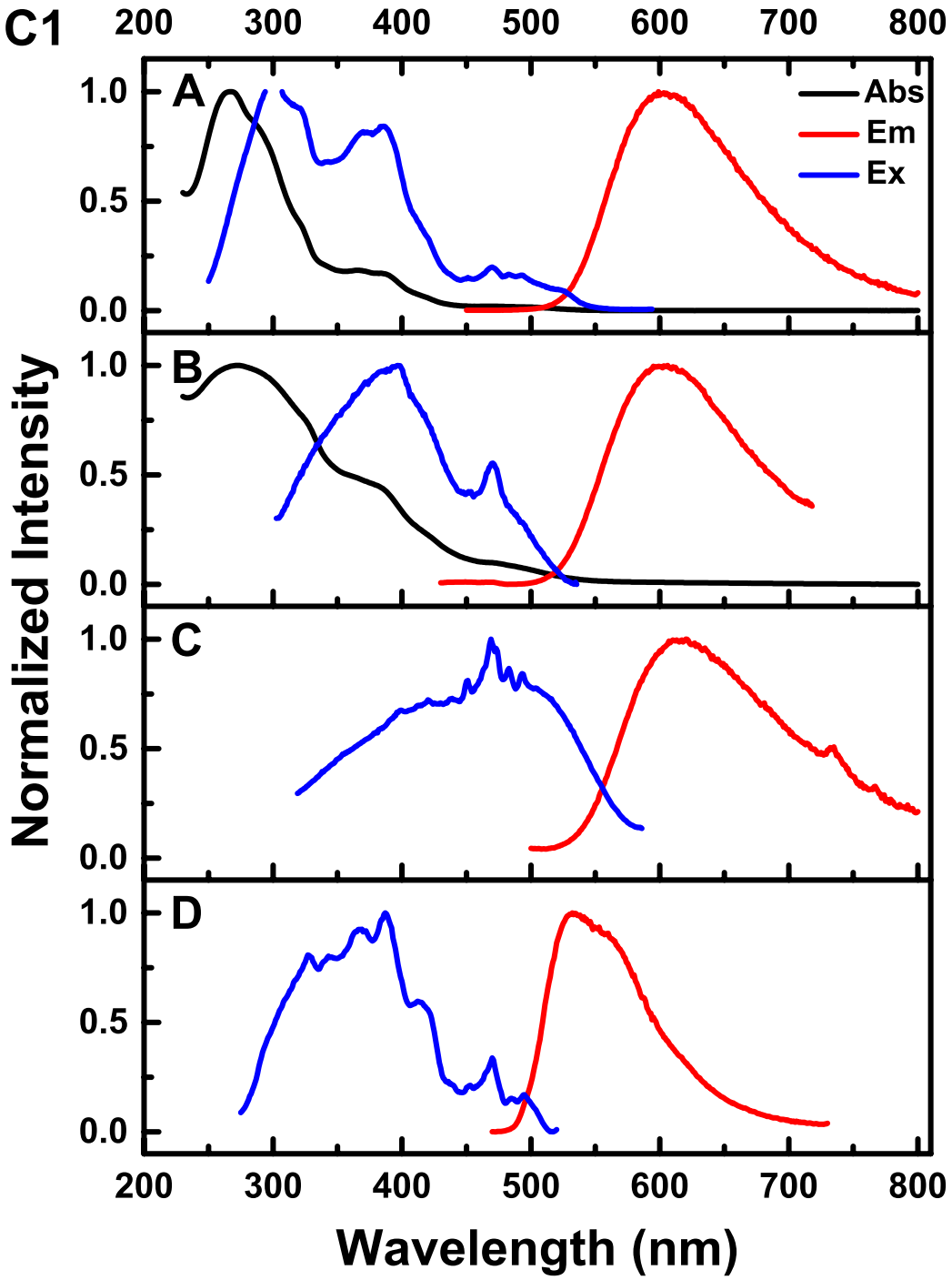

Fig. S12 Absorbance (black), photoluminescence excitation (blue), and emission (red) spectra of **C1**. A) Solution: DCM, 298 K, a 380 UV longpass optical filter was used for this emission profile; B) Dropcast Film: Evaporated from a concentrated solution in DCM, 298 K; C) Solid: 298 K; D) Frozen: 2-MeTHF, 77 K. The break in the solution excitation spectrum signifies an omitted peak due to half the emission wavelength. Both the broad, featureless emission peaks (red) and the rigidochromic effect present in the frozen state (D) are indicative of MLCT emission.

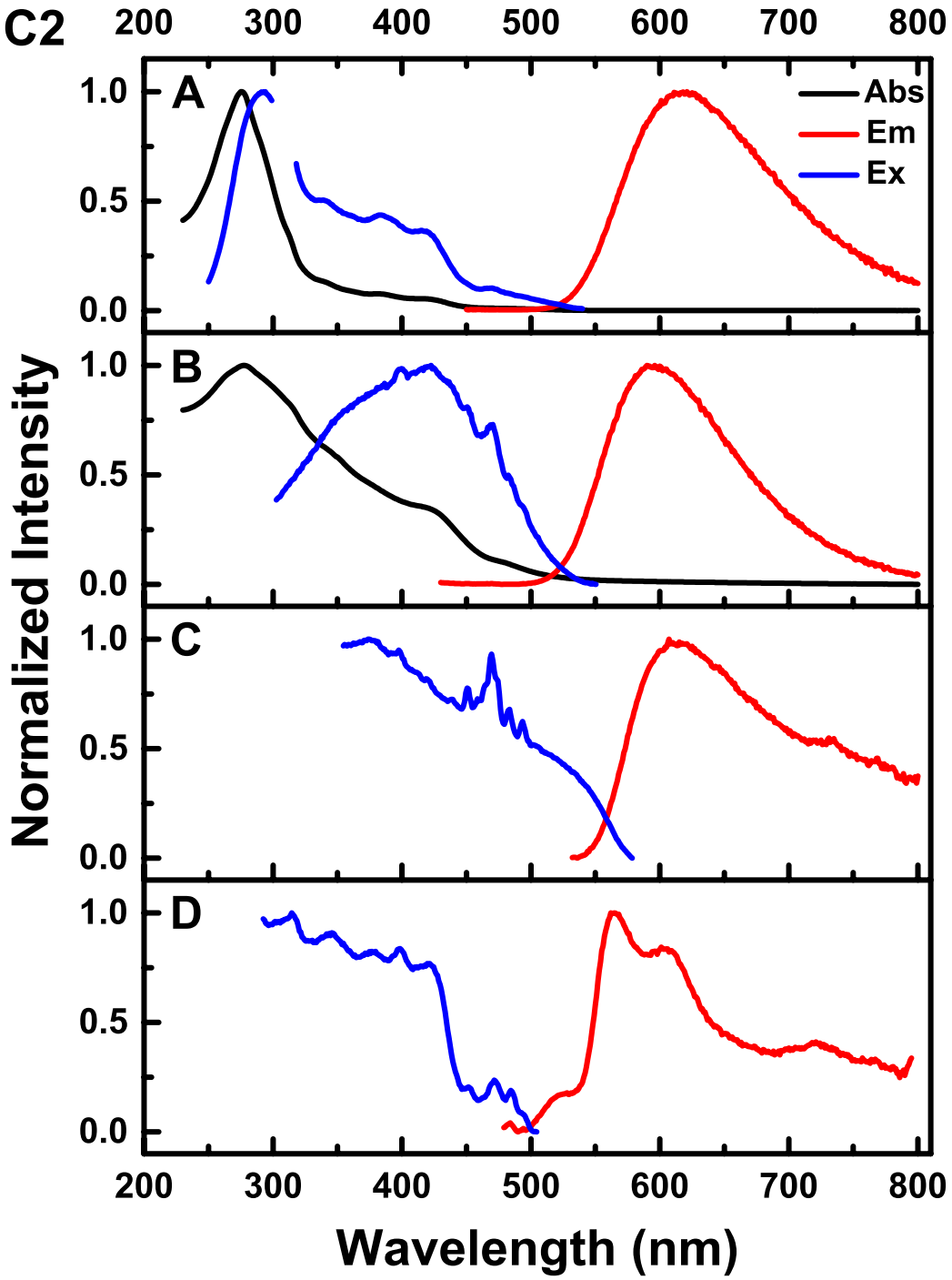

Fig. S13 Absorbance (black), photoluminescence excitation (blue), and emission (red) spectra of **C2**. A) Solution: DCM, 298 K, a 380 UV longpass optical filter was used for this emission profile; B) Dropcast Film: Evaporated from a concentrated solution in DCM, 298 K; C) Solid: 298 K; D) Frozen: 2-MeTHF, 77 K. The break in the solution excitation spectrum signifies an omitted peak due to half the emission wavelength. Both the broad, featureless emission peaks (red) and the rigidochromic effect present in the frozen state (D) are indicative of MLCT emission.

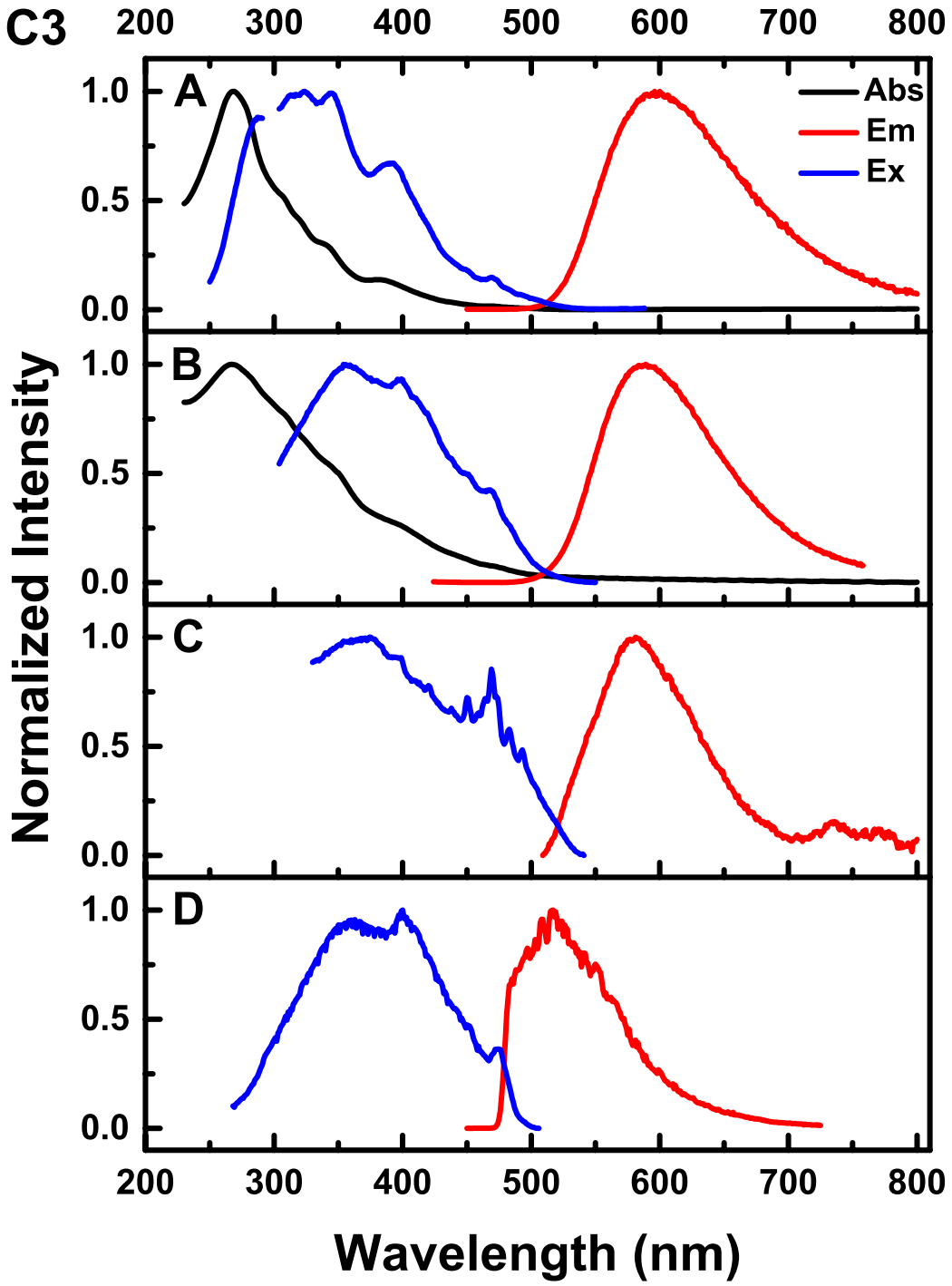

Fig. S14 Absorbance (black), photoluminescence excitation (blue), and emission (red) spectra of **C3**. A) Solution: DCM, 298 K, a 380 UV longpass optical filter was used for this emission profile; B) Dropcast Film: Evaporated from a concentrated solution in DCM, 298 K; C) Solid: 298 K; D) Frozen: 2-MeTHF, 77 K. The break in the solution excitation spectrum signifies an omitted peak due to half the emission wavelength. Both the broad, featureless emission peaks (red) and the rigidochromic effect present in the frozen state (D) are indicative of MLCT emission.

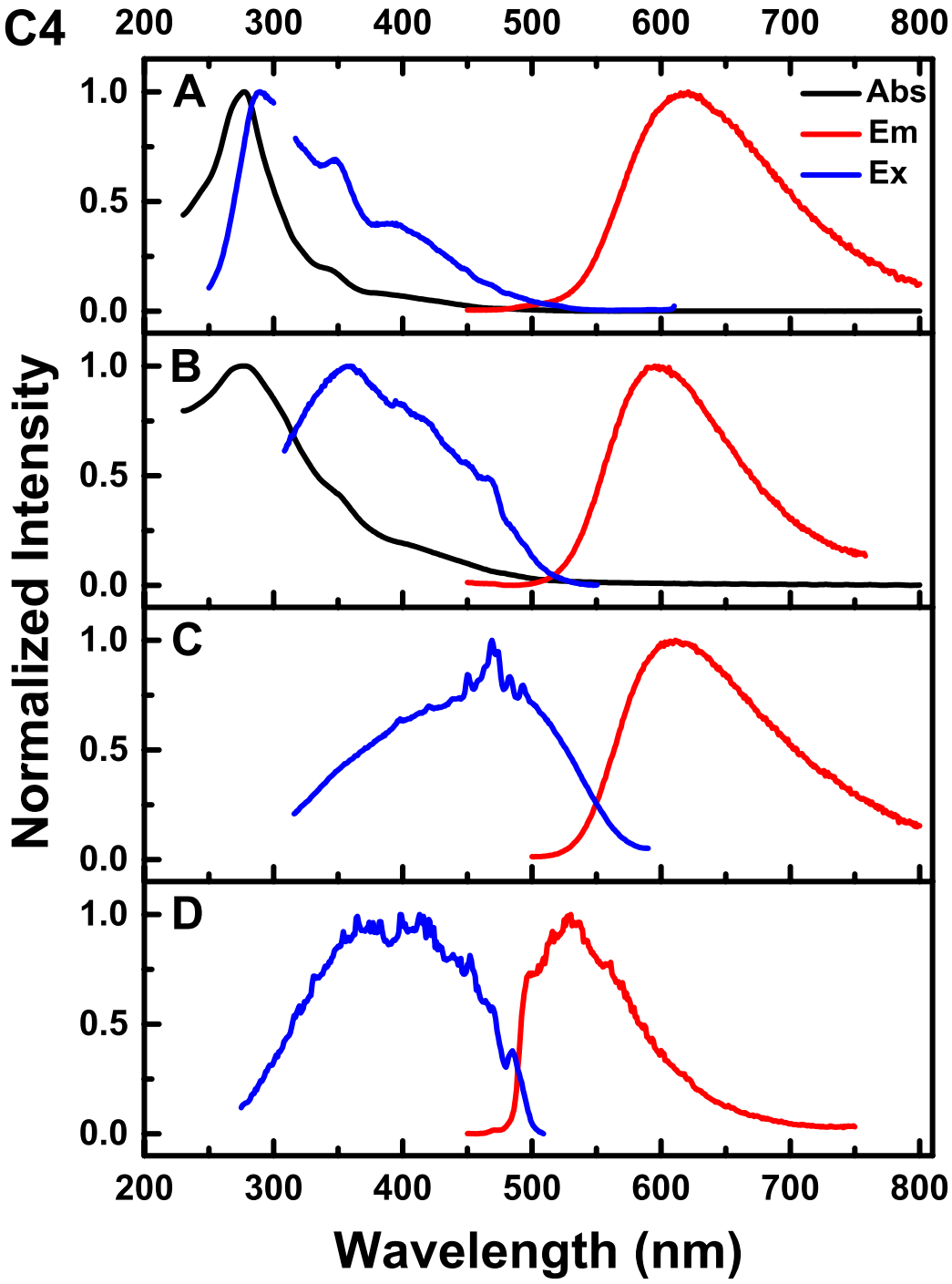

Fig. S15 Absorbance (black), photoluminescence excitation (blue), and emission (red) spectra of **C4**. A) Solution: DCM, 298 K, a 380 UV longpass optical filter was used for this emission profile; B) Dropcast Film: Evaporated from a concentrated solution in DCM, 298 K; C) Solid: 298 K; D) Frozen: 2-MeTHF, 77 K. The break in the solution excitation spectrum signifies an omitted peak due to half the emission wavelength. Both the broad, featureless emission peaks (red) and the rigidochromic effect present in the frozen state (D) are indicative of MLCT emission.

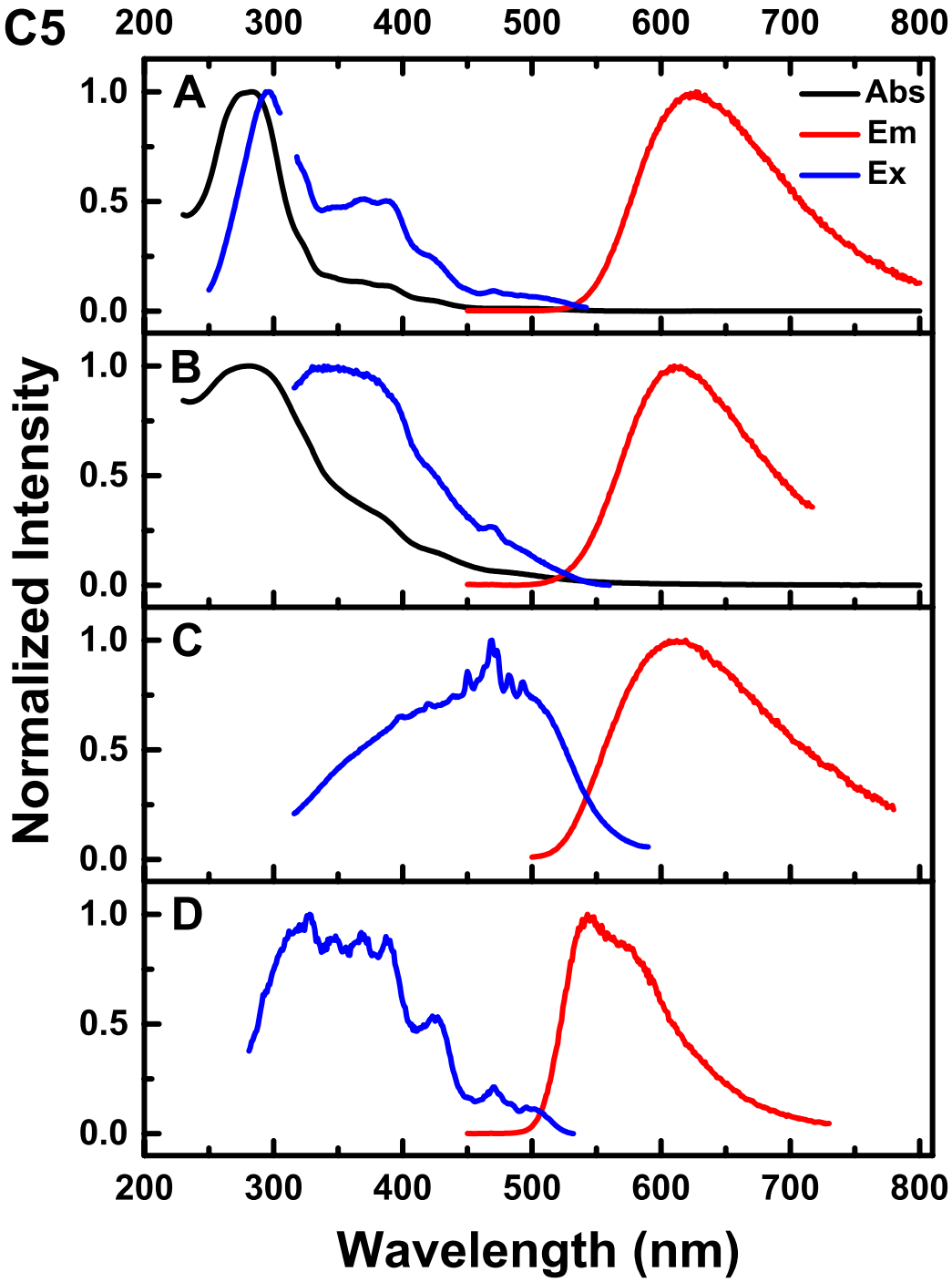

Fig. S16 Absorbance (black), photoluminescence excitation (blue), and emission (red) spectra of **C5**. A) Solution: DCM, 298 K, a 380 UV longpass optical filter was used for this emission profile; B) Dropcast Film: Evaporated from a concentrated solution in DCM, 298 K; C) Solid: 298 K; D) Frozen: 2-MeTHF, 77 K. The break in the solution excitation spectrum signifies an omitted peak due to half the emission wavelength. Both the broad, featureless emission peaks (red) and the rigidochromic effect present in the frozen state (D) are indicative of MLCT emission.

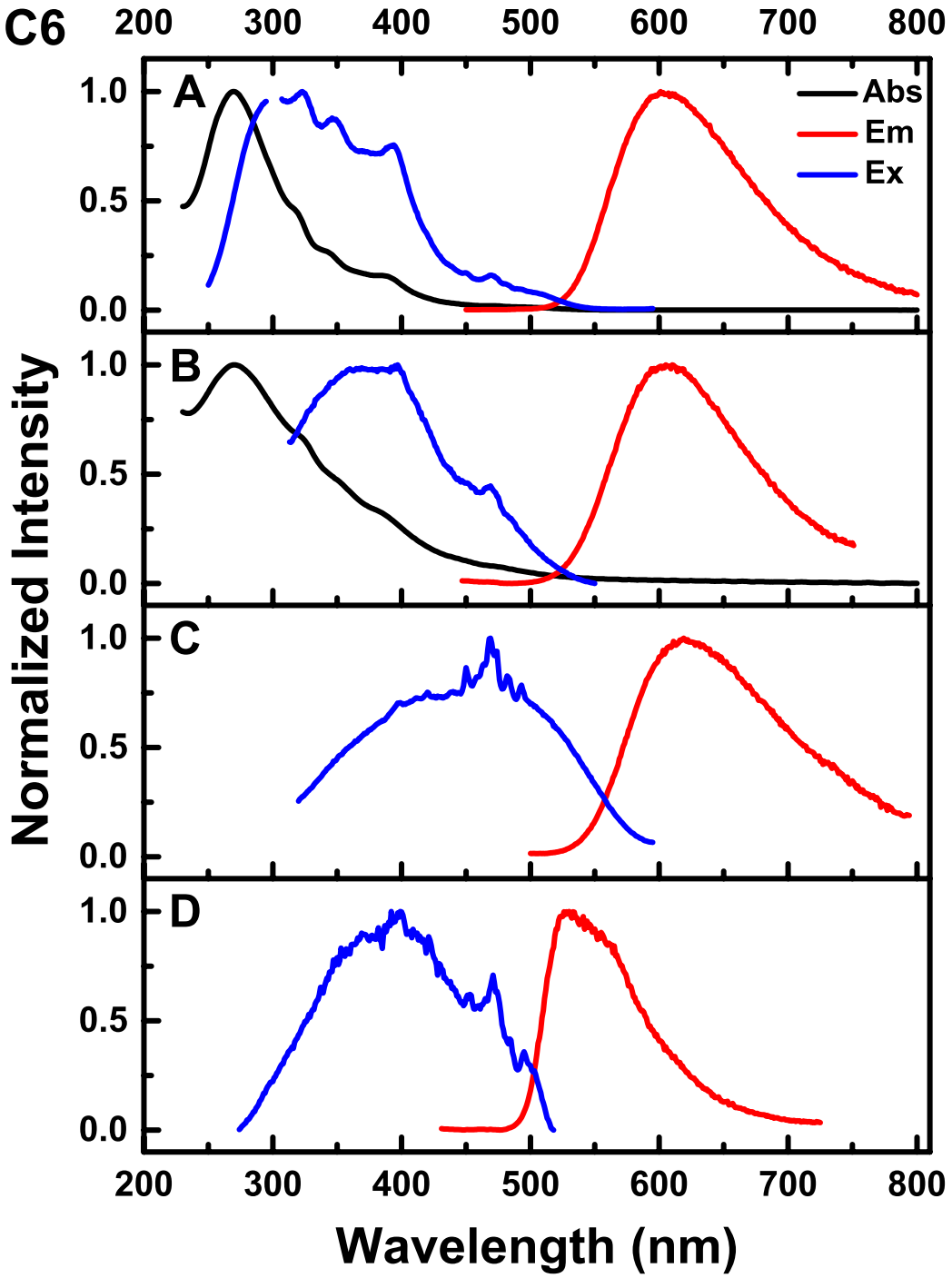

Fig. S17 Absorbance (black), photoluminescence excitation (blue), and emission (red) spectra of **C6**. A) Solution: DCM, 298 K, a 380 UV longpass optical filter was used for this emission profile; B) Dropcast Film: Evaporated from a concentrated solution in DCM, 298 K; C) Solid: 298 K; D) Frozen: 2-MeTHF, 77 K. The break in the solution excitation spectrum signifies an omitted peak due to half the emission wavelength. Both the broad, featureless emission peaks (red) and the rigidochromic effect present in the frozen state (D) are indicative of MLCT emission.

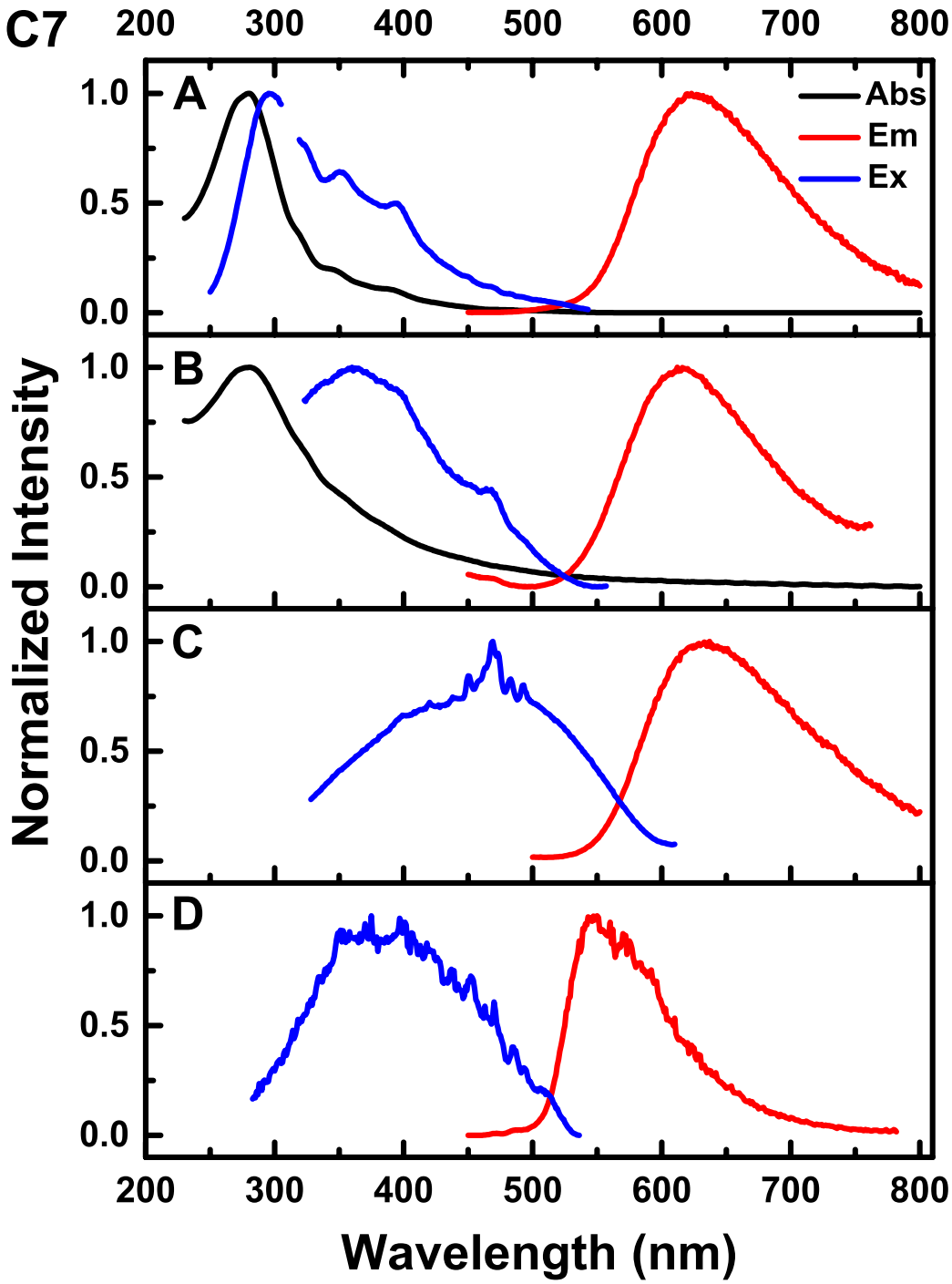

Fig. S18 Absorbance (black), photoluminescence excitation (blue), and emission (red) spectra of **C7**. A) Solution: DCM, 298 K, a 380 UV longpass optical filter was used for this emission profile; B) Dropcast Film: Evaporated from a concentrated solution in DCM, 298 K; C) Solid: 298 K; D) Frozen: 2-MeTHF, 77 K. The break in the solution excitation spectrum signifies an omitted peak due to half the emission wavelength. Both the broad, featureless emission peaks (red) and the rigidochromic effect present in the frozen state (D) are indicative of MLCT emission.

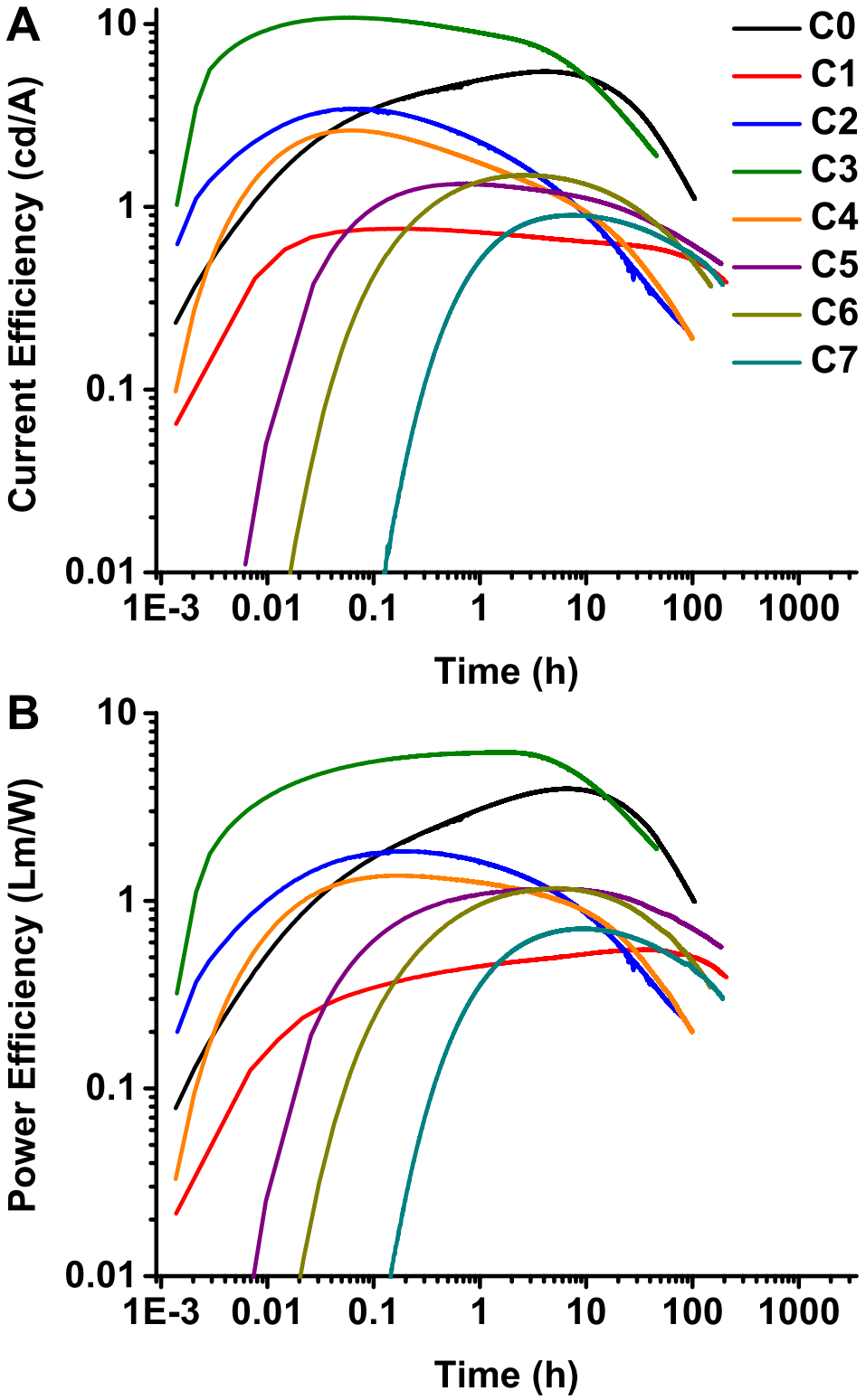

Fig. S19: A) Current efficiency vs. time and B) power efficiency vs. time of **C0–C7** LEEC devices with 0.3% $LIPF_6$. Plotted with a logarithmic scale on the x- and y-axes to more easily visualize the plot maxima.

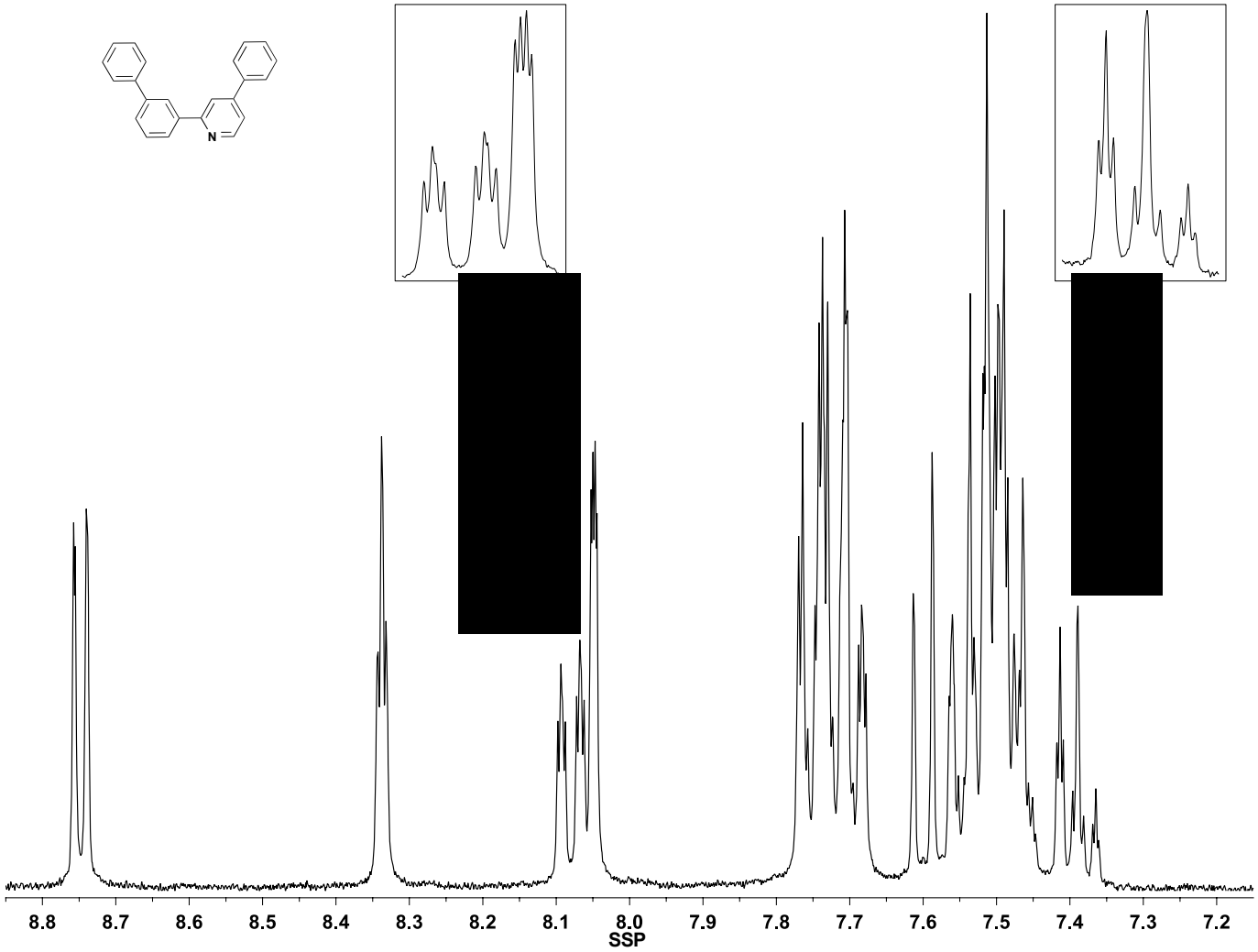

Fig. S20 ^{1}H NMR spectrum of **BiPhPhPy** in CD_2Cl_2 at 300 MHz. Insets: Expanded regions to show convoluted secondary coupling patterns denoted by a tilde (~). 8.75 (dd, J = 5.1, 0.9, 1H), 8.34 (t, J = 1.7, 1H), 8.08 (dt, J = 7.7, 1.4, 1H), 8.05 (~s, 1H), 7.72 (m, 5H), 7.49 (m, 7H), 7.39 (~t, J = 7.4, 1H).

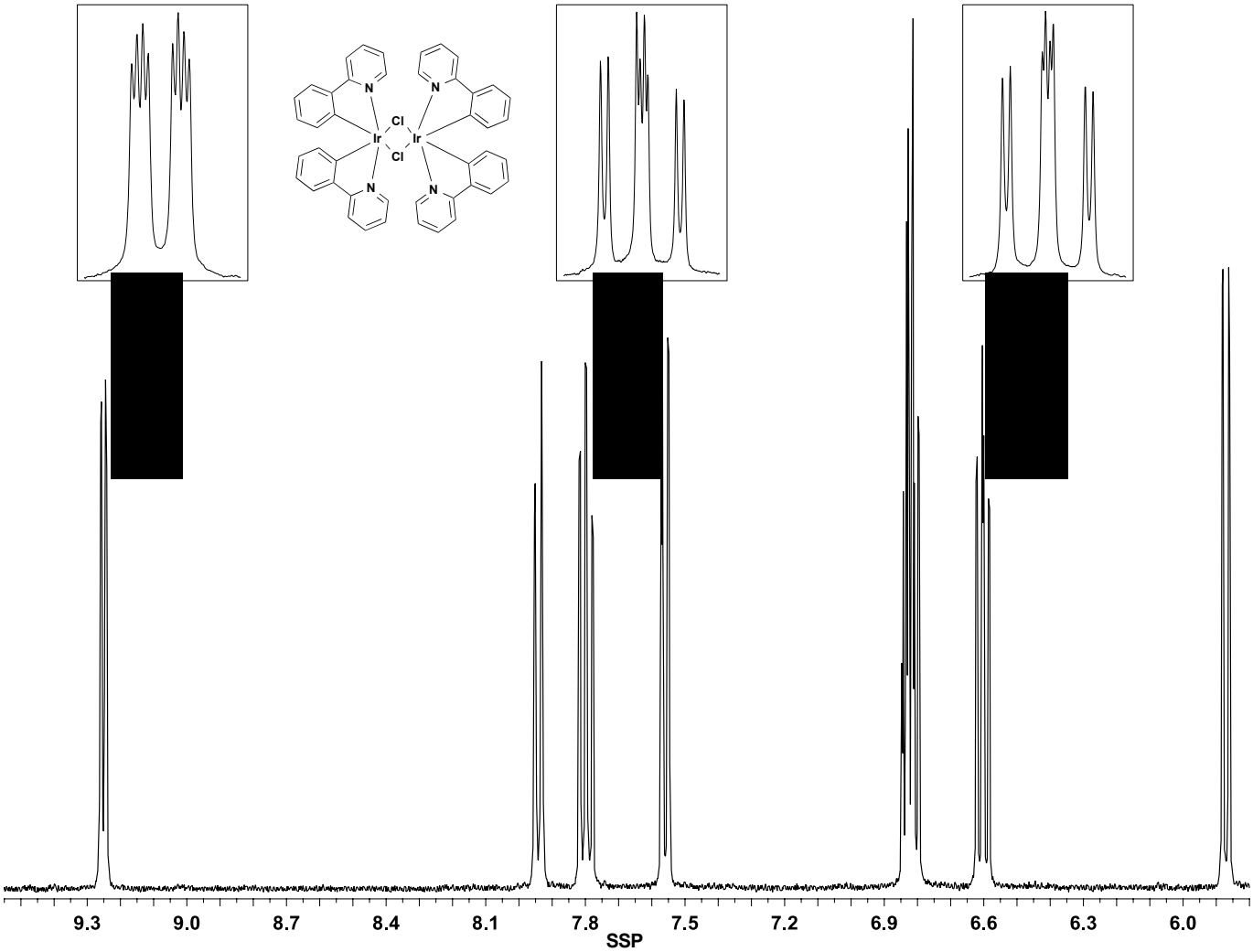

Fig. S21 ^{1}H NMR spectrum of **D1** in CD_2Cl_2 at 400 MHz. Insets: Expanded regions to show convoluted secondary coupling patterns denoted by a tilde (~). 9.25 (~d, J = 5.8, 4H), 7.94 (d, J = 7.8, 4H), 7.80 (~t, J = 7.8, 4H), 7.56 (dd, J = 7.8, 1.4, 4H), 6.82 (m, 8H), 6.60 (~t, J = 7.6, 4H), 5.87 (dd, J = 7.6, 0.8, 4H).

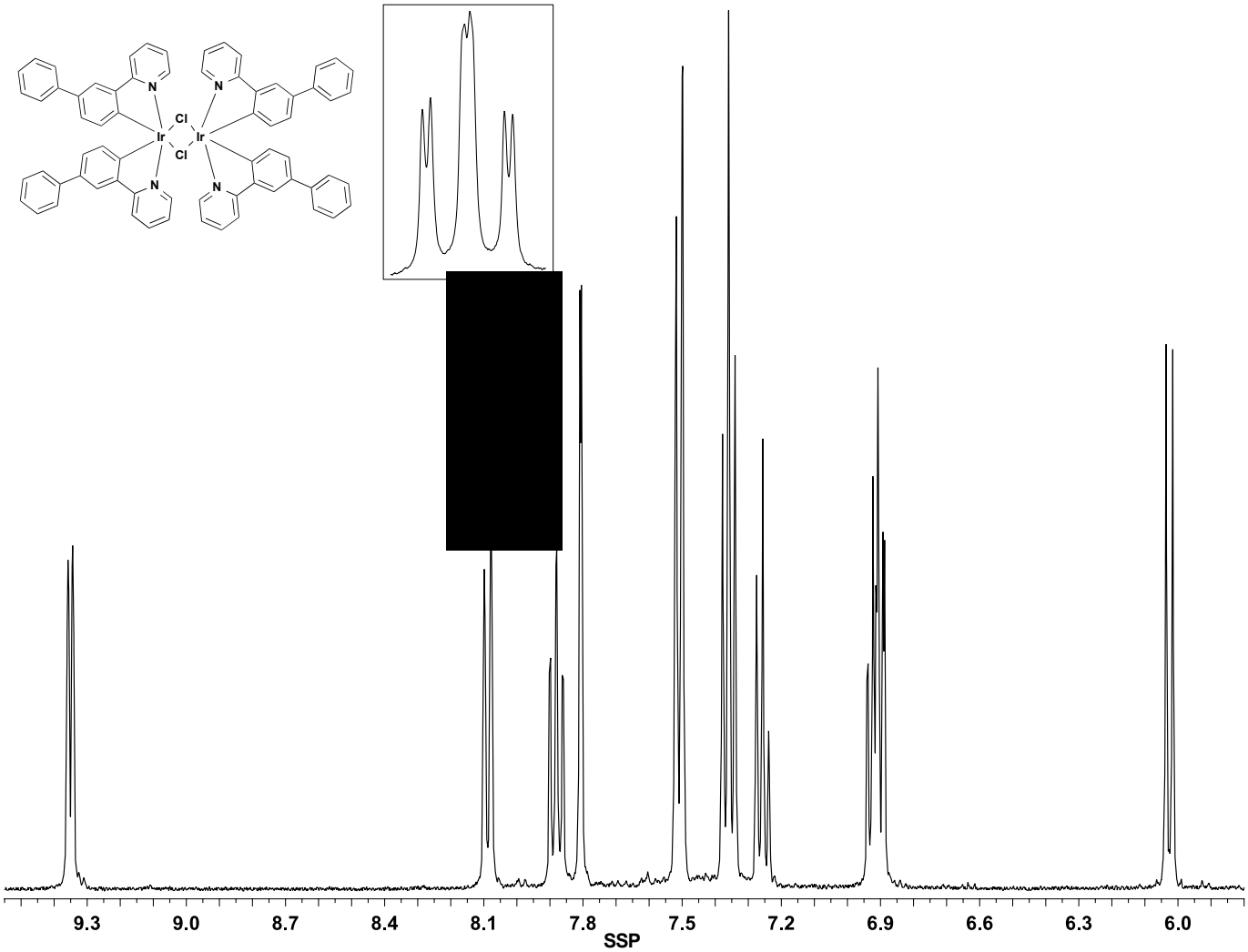

Fig. S22 ^{1}H NMR spectrum of **D2** in CD_2Cl_2 at 400 MHz. Insets: Expanded regions to show convoluted secondary coupling patterns denoted by a tilde (~). 9.35 (d, J = 5.6, 4H), 8.09 (d, J = 8.0, 4H), 7.88 (~t, J = 7.9, 4H), 7.81 (d, J = 2.0, 4H), 7.51 (d, J = 8.0, 8H), 7.36 (t, J = 7.8, 8H), 7.26 (t, J = 7.2, 4H), 6.91 (m, 8H), 6.03 (d, J = 8.4, 4H).

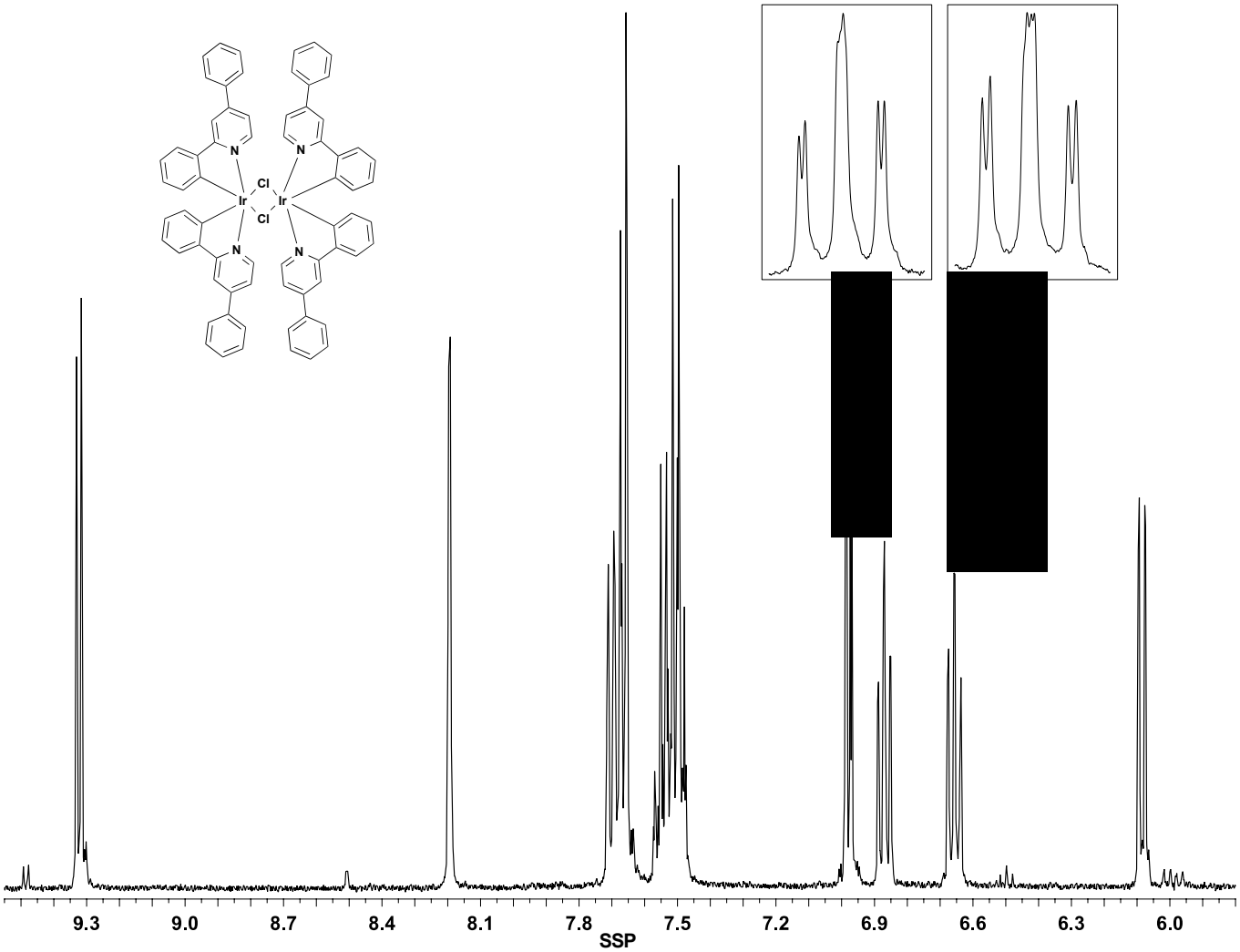

Fig. S23 ^{1}H NMR spectrum of **D3** in CD_2Cl_2 at 400 MHz. Insets: Expanded regions to show convoluted secondary coupling patterns denoted by a tilde (~). 9.32 (d, J = 5.6, 4H), 8.19 (d, J = 2.0, 4H), 7.67 (m, 12H), 7.52 (m, 12H), 6.98 (dd, J = 6.4, 2.0, 4H), 6.87 (~t, J = 7.4, 4H), 6.66 (~t, J = 7.4, 4H), 6.09 (dd, J = 7.8, 1.0, 4H).

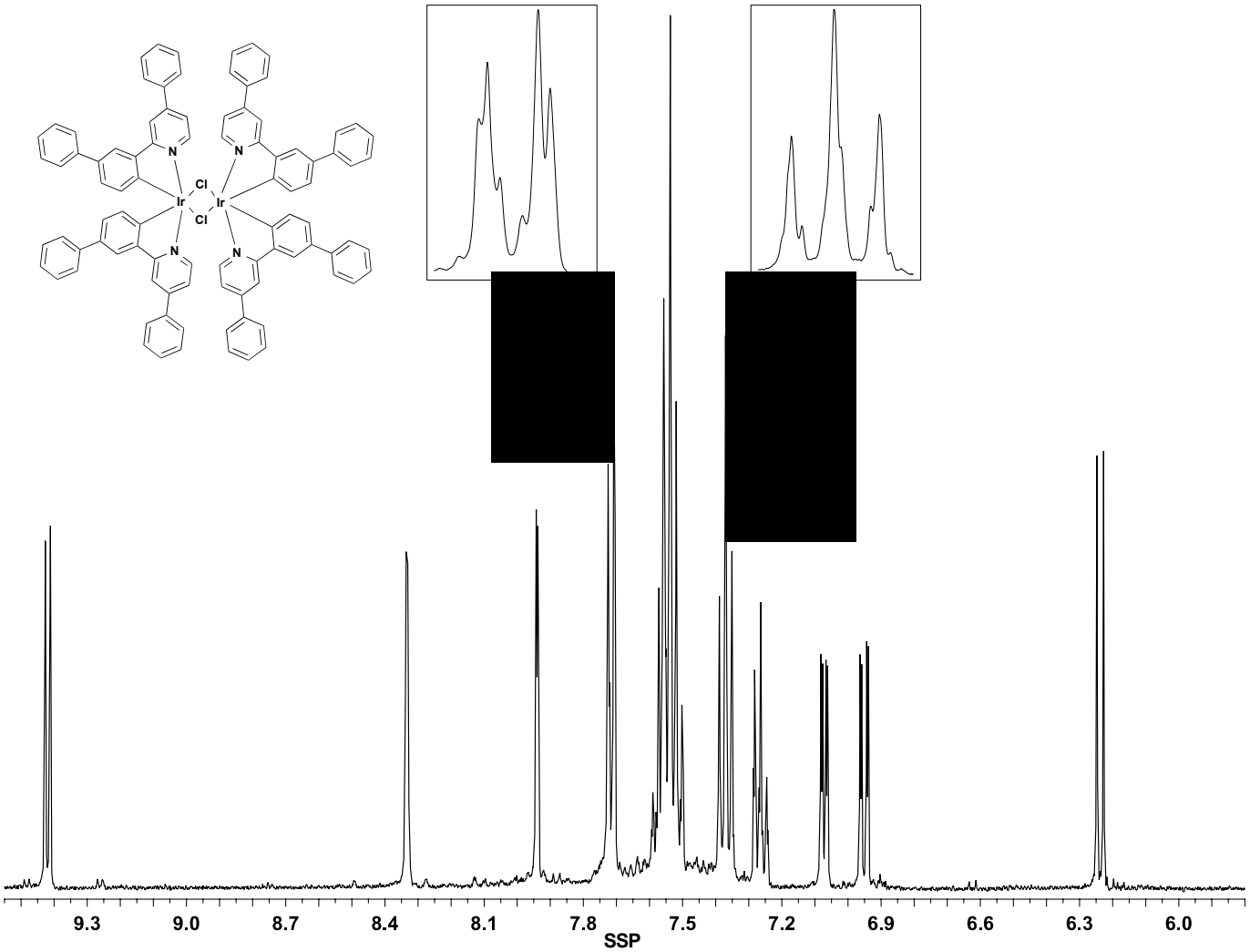

Fig. S24 ^{1}H NMR spectrum of **D4** in CD_2Cl_2 at 400 MHz. Insets: Expanded regions to show convoluted secondary coupling patterns denoted by a tilde (~). 9.42 (d, J = 6.0, 4H), 8.33 (d, J = 2.0, 4H), 7.94 (d, J = 2.0, 4H), 7.72 (~d, J = 7.8, 8H), 7.55 (m, 20H), 7.37 (~t, J = 7.6, 8H), 7.26 (tt, J = 7.4, 1.4, 4H), 7.07 (dd, J = 6.2, 2.2, 4H), 6.95 (dd, J = 8.0, 2.0, 4H), 6.24 (d, J = 8.0, 4H).

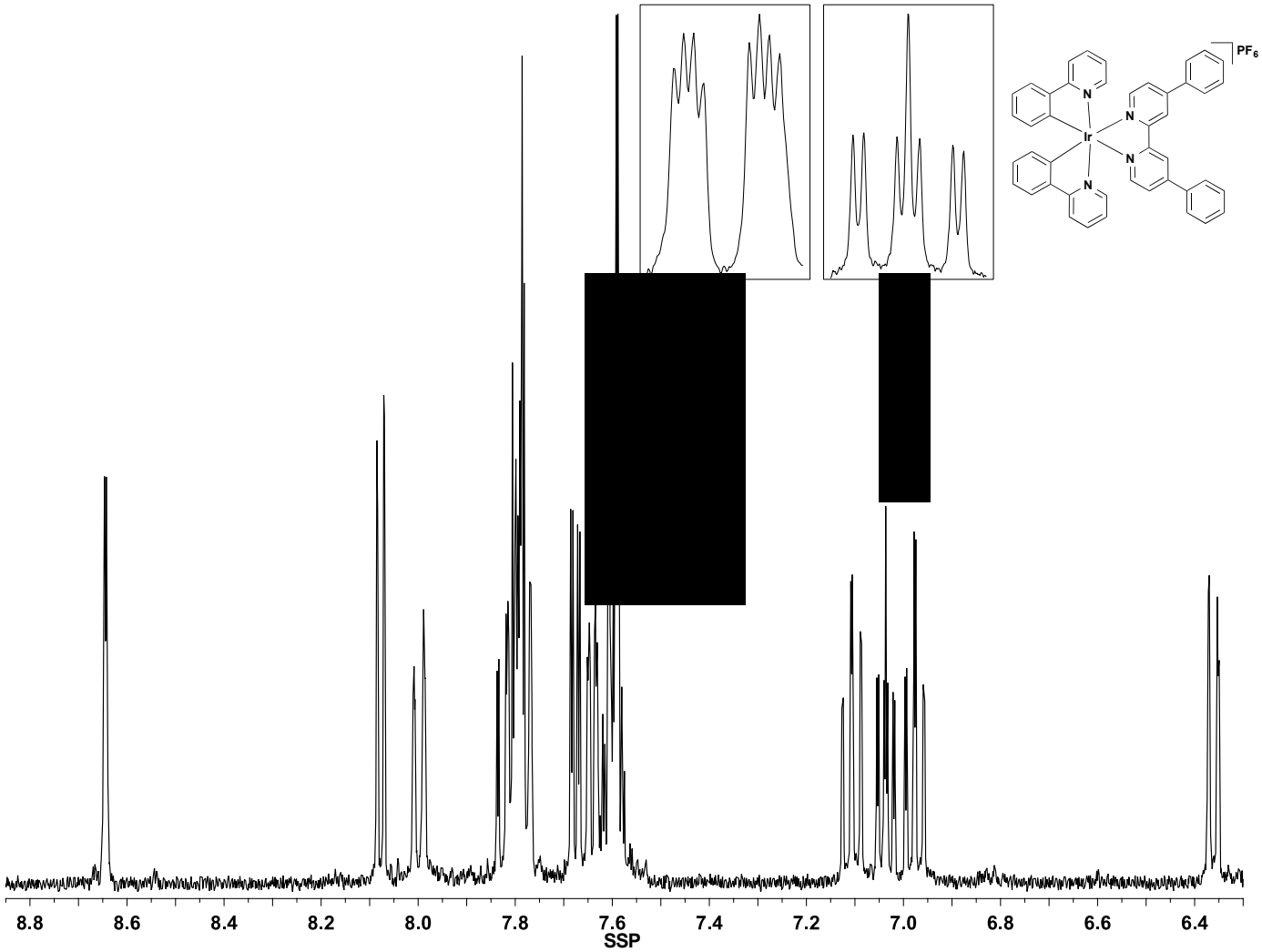

Fig. S25 ^{1}H NMR spectrum of **C1** in CD_2Cl_2 at 400 MHz. Insets: Expanded regions to show convoluted secondary coupling patterns denoted by a tilde (~). 8.64 (d, *J* = 1.6, 2H), 8.08 (d, *J* = 6.0, 2H), 8.00 (d, *J* = 8.4, 2H), 7.80 (m, 8H), 7.68 (dd, *J* = 5.8, 1.8, 2H), 7.64 (~d, *J* = 6.0, 2H), 7.60 (m, 6H), 7.11 (td, *J* = 7.6, 1.2, 2H), 7.04 (~t, *J* = 6.7, 2H), 6.98 (td, *J* = 7.4, 1.3, 2H), 6.36 (dd, *J* = 8.0, 0.8, 2H).

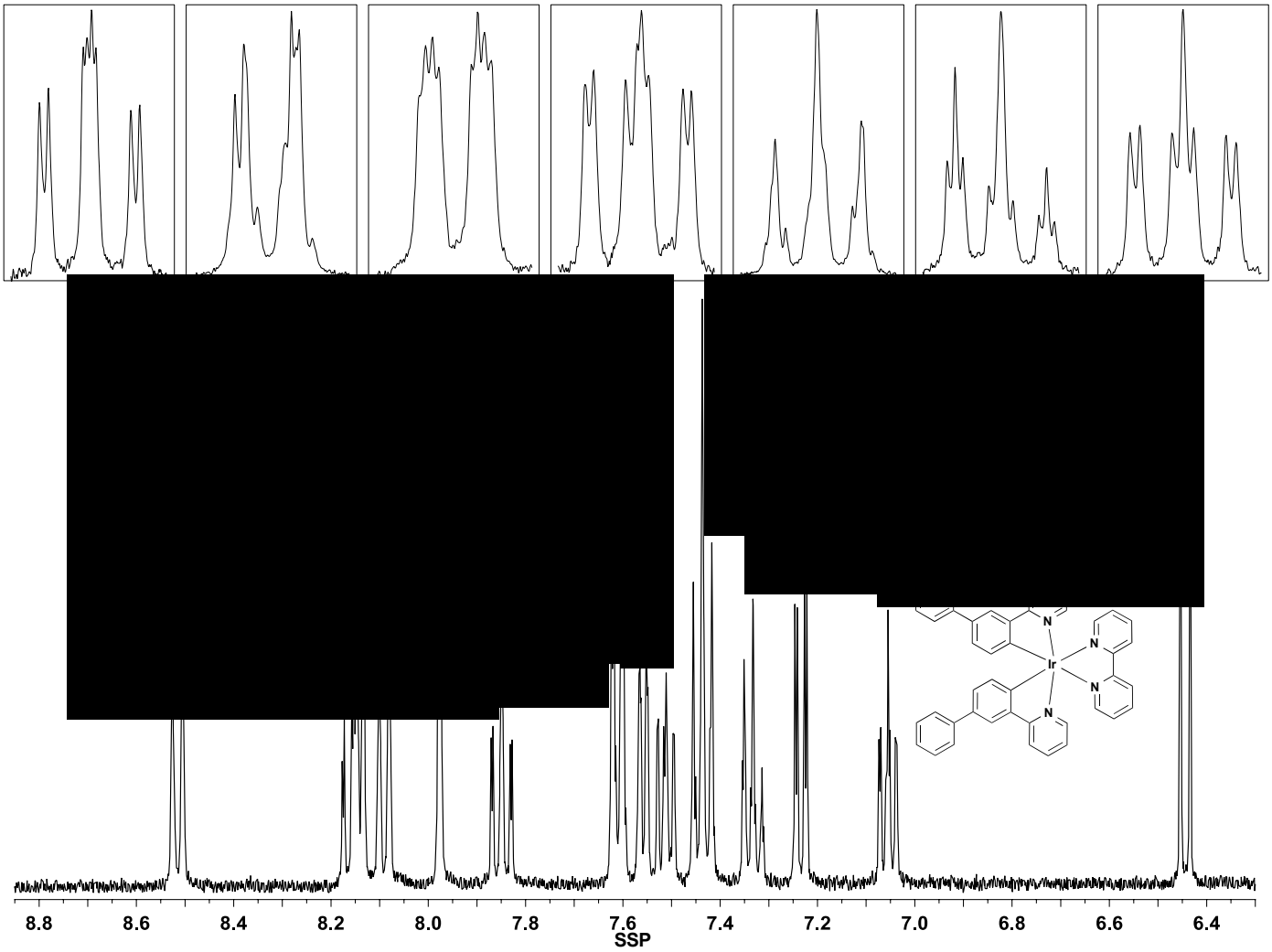

Fig. S26 ^{1}H NMR spectrum of **C2** in CD_2Cl_2 at 400 MHz. Insets: Expanded regions to show convoluted secondary coupling patterns denoted by a tilde (~). 8.52 (d, *J* = 8.0, 2H), 8.16 (m, 4H), 8.09 (d, *J* = 8.0, 2H), 7.98 (d, *J* = 2.0, 2H), 7.85 (~t, *J* = 7.8, 2H), 7.61 (~d, *J* = 8.4, 4H), 7.56 (~d, *J* = 5.6, 2H), 7.51 (~t, *J* = 6.6, 2H), 7.44 (~t, *J* = 7.4, 4H), 7.33 (~t, *J* = 7.4, 2H), 7.23 (dd, *J* = 7.6, 2.0, 2H), 7.06 (~t, *J* = 6.8, 2H), 6.44 (d, *J* = 8.0, 2H).

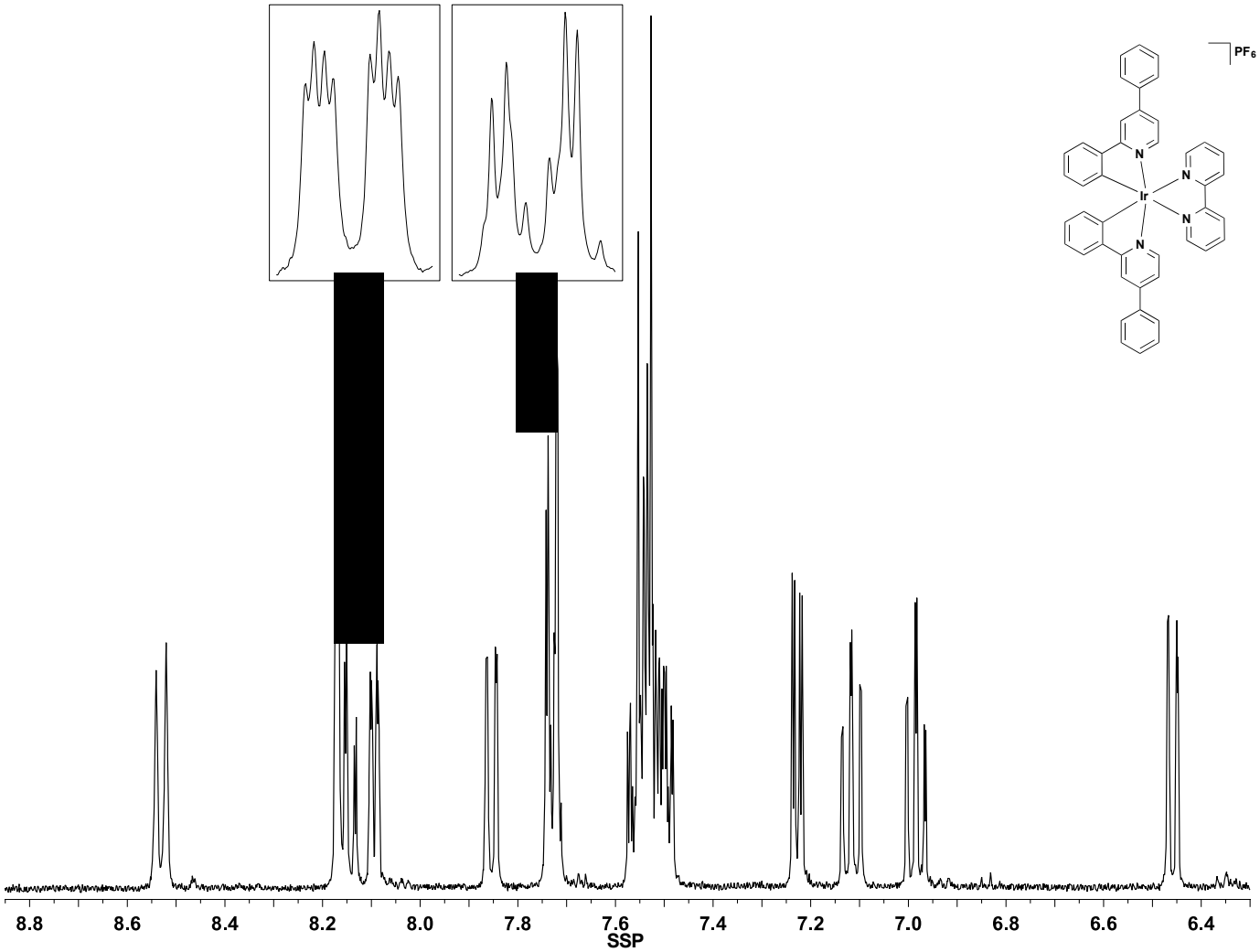

Fig. S27 ^{1}H NMR spectrum of **C3** in CD_2Cl_2 at 400 MHz. Insets: Expanded regions to show convoluted secondary coupling patterns denoted by a tilde (~). 8.53 (d, *J* = 8.0, 2H), 8.15 (m, 4H), 8.09 (~d, *J* = 5.4, 2H), 7.85 (dd, *J* = 7.6, 1.2, 2H), 7.73 (~d, *J* = 8.2, 4H), 7.53 (m, 10H), 7.23 (dd, *J* = 6.0, 2.0, 2H), 7.12 (td, *J* = 7.4, 1.2, 2H), 6.99 (td, *J* = 7.5, 1.3, 2H), 6.46 (dd, *J* = 7.6, 0.8, 2H).

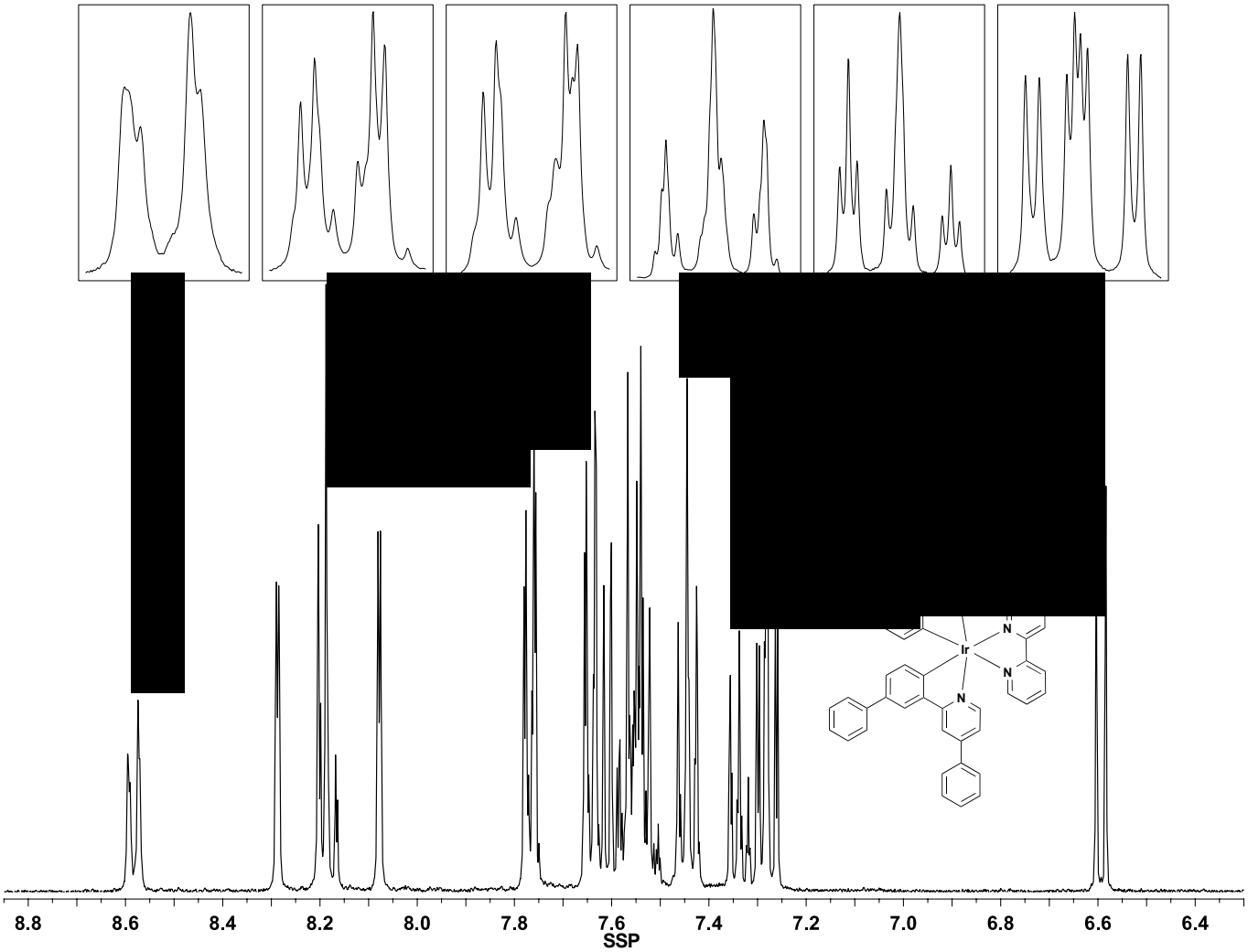

Fig. S28 ^{1}H NMR spectrum of **C4** in CD_2Cl_2 at 400 MHz. Insets: Expanded regions to show convoluted secondary coupling patterns denoted by a tilde (~). 8.58 (~d, *J* = 8.2, 2H), 8.29 (d, *J* = 2.0, 2H), 8.18 (m, 4H), 8.08 (d, *J* = 2.0, 2H), 7.77 (~d, *J* = 8.2, 4H), 7.64 (~d, *J* = 8.4, 4H), 7.61 (d, *J* = 6.4, 2H), 7.55 (m, 8H), 7.44 (~t, *J* = 7.6, 4H), 7.34 (~t, *J* = 7.2, 2H), 7.28 (~t, *J* = 7.6, 4H), 6.59 (d, *J* = 8.0, 2H).

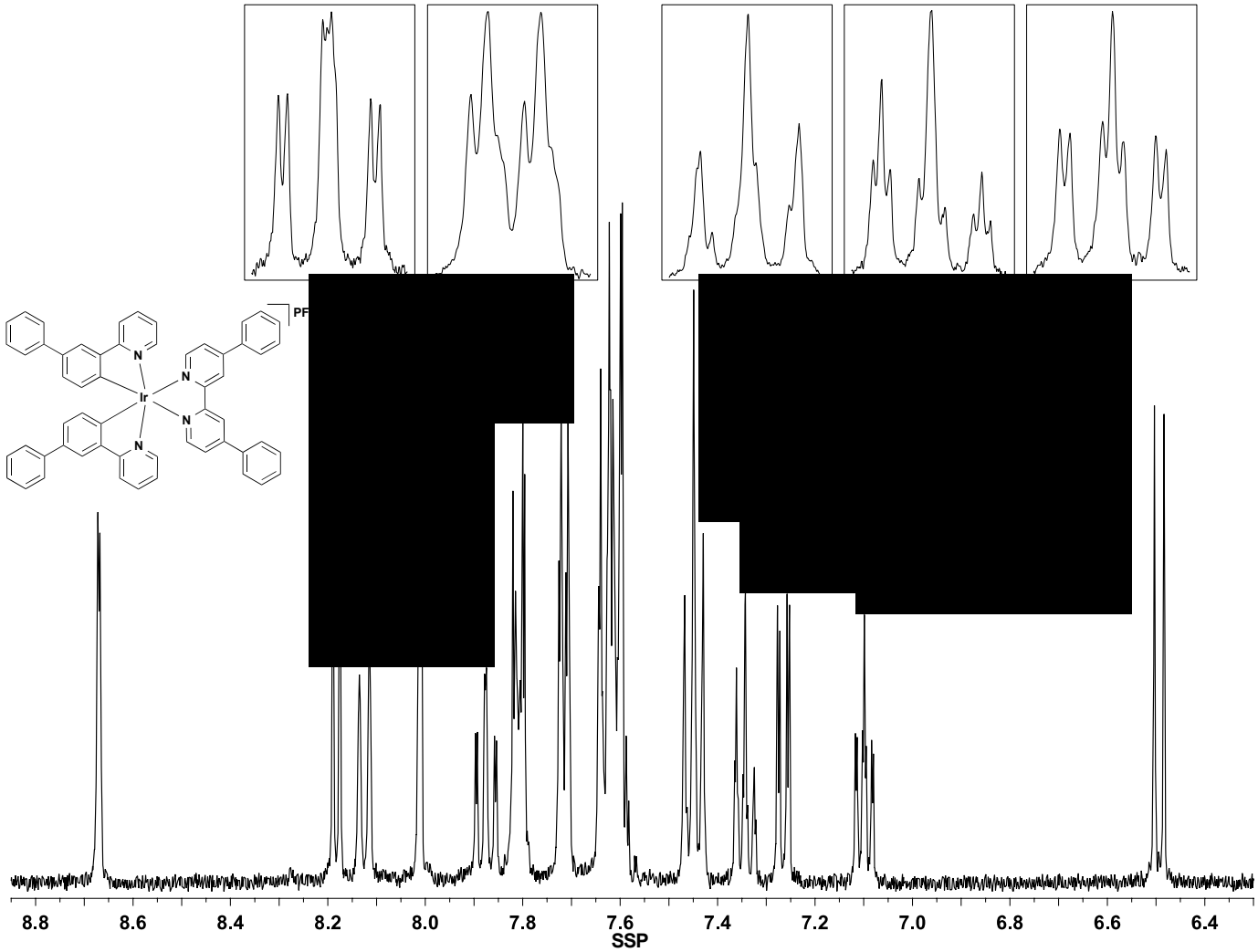

Fig. S29 ^{1}H NMR spectrum of **C5** in CD_2Cl_2 at 400 MHz. Insets: Expanded regions to show convoluted secondary coupling patterns denoted by a tilde (~). 8.67 (d, *J* = 1.6, 2H), 8.18 (d, *J* = 5.6, 2H), 8.13 (d, *J* = 8.0, 2H), 8.01 (d, *J* = 2.0, 2H), 7.88 (~t, *J* = 7.8, 2H), 7.81 (m, 4H), 7.72 (~d, *J* = 6.0, 4H), 7.61 (m, 10H), 7.45 (~t, *J* = 7.6, 4H), 7.34 (~t, *J* = 7.2, 2H), 7.27 (dd, *J* = 8.0, 2.0, 2H), 7.10 (~t, *J* = 6.7, 2H), 6.49 (d, *J* = 8.0, 2H).

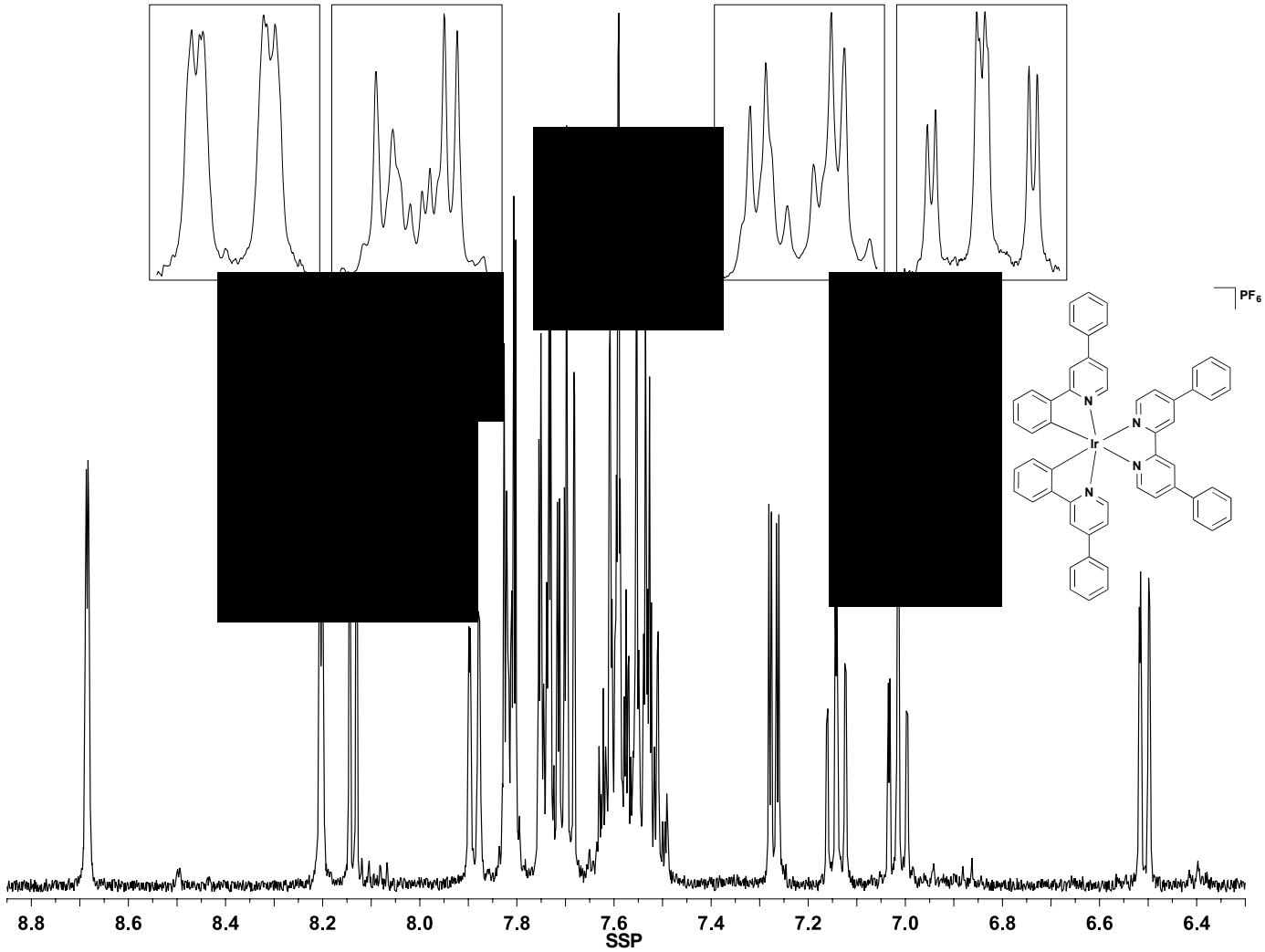

Fig. S30 ^{1}H NMR spectrum of **C6** in CD_2Cl_2 at 400 MHz. Insets: Expanded regions to show convoluted secondary coupling patterns denoted by a tilde (~). 8.69 (d, *J* = 1.6, 2H), 8.20 (d, *J* = 2.0, 2H), 8.14 (d, *J* = 5.6, 2H), 7.89 (~d, *J* = 7.6, 2H), 7.82 (~d, *J* = 8.0, 4H), 7.74 (~d, *J* = 8.2, 4H), 7.70 (m, 4H), 7.56 (m, 12H), 7.27 (dd, *J* = 6.0, 2.0, 2H), 7.14 (~t, *J* = 7.6, 2H), 7.02 (td, *J* = 7.4, 1.2, 2H), 6.51 (dd, *J* = 7.6, 0.8, 2H).

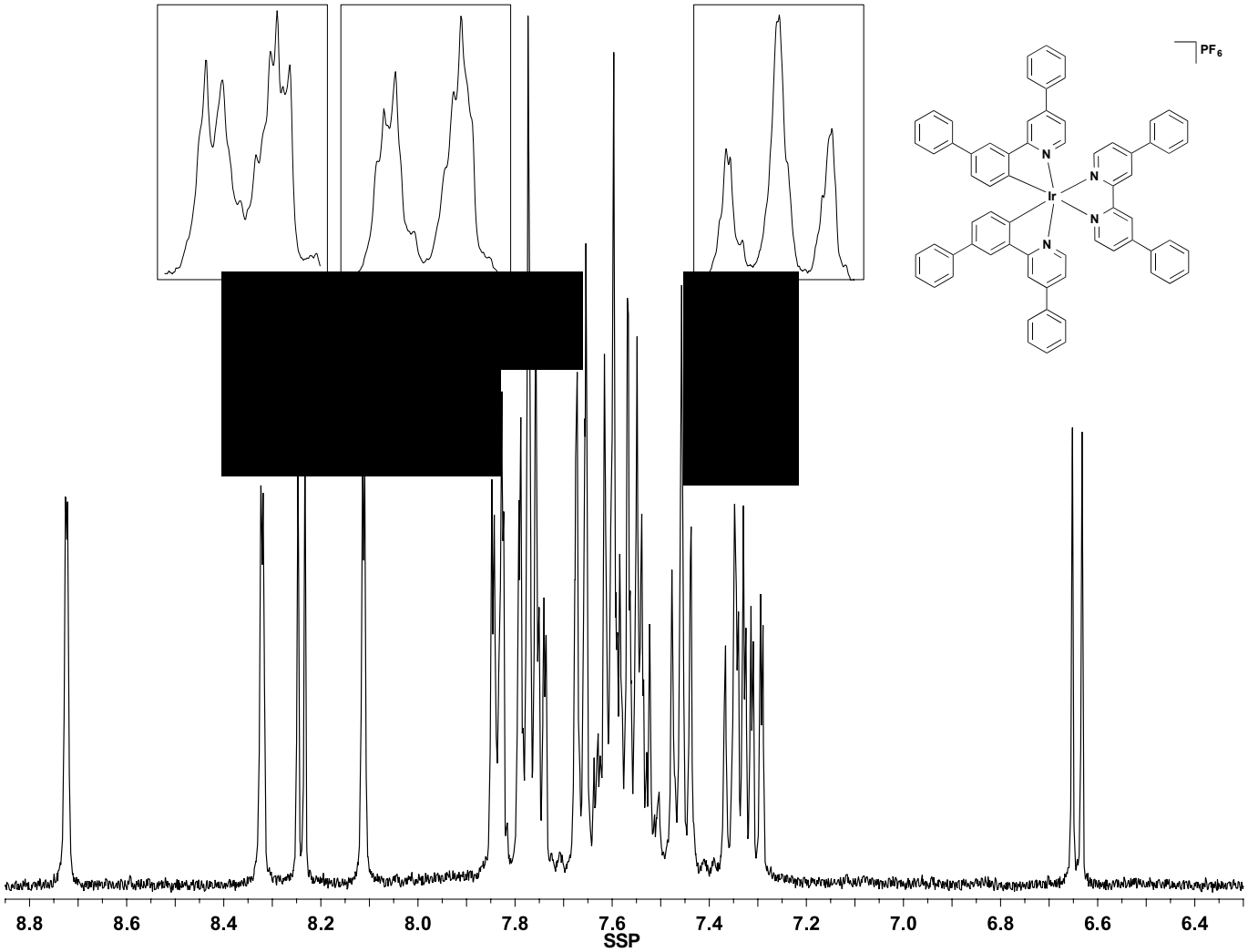

Fig. S31 ^{1}H NMR spectrum of **C7** in CD_2Cl_2 at 400 MHz. Insets: Expanded regions to show convoluted secondary coupling patterns denoted by a tilde (~). 8.72 (d, J = 1.6, 2H), 8.32 (d, J = 2.0, 2H), 8.24 (d, J = 6.0, 2H), 8.11 (d, J = 2.0, 2H), 7.84 (~d, J = 8.0, 4H), 7.77 (m, 8H), 7.67 (~d, J = 7.2, 4H), 7.57 (m, 12H), 7.46 (~t, J = 7.8, 4H), 7.33 (m, 6H), 6.64 (d, J = 7.6, 2H).